https://dx.doi.org/10.1016/j.cemconres.2022.106891

Preparation aragonite whisker-rich materials by wet carbonation of cement: towards yielding micro-fiber reinforced cement and sequestrating CO_2

Peiliang Shen [a], Jianxin Lu [a], Yangyang Zhang [b],
Yi Jiang [a], Shipeng Zhang [a] *, Chi Sun Poon [a] *

[a] Department of Civil and Environmental Engineering, Research Centre for Resources Engineering toward Carbon Neutrality, The Hong Kong Polytechnic University, Hung Hom, Kowloon, Hong Kong

[b] School of Civil Engineering and Mechanics, Yanshan University, Qinhuangdao, Hebei, China

*Corresponding author, cecspoon@polyu.edu.hk (C.S. Poon)

*Corresponding author, shipeng.zhang@polyu.edu.hk (Shipeng Zhang)

Abstract: In this study, an innovative wet carbonation process was developed to prepare aragonite whisker-rich materials (AWM) from cement and simulated flue gas, which subsequently served as micro-fiber additions to cement. The parameters including temperature, duration and $MgCl_2$ concentration governing the aragonite formation were investigated, and the formation mechanism was explored. The results showed that needle-like aragonite whisker with a single crystal length of 10-30 μm and diameter of 0.5-2 μm could be synthesized rapidly when the cement suspension containing 0.05 M/L $MgCl_2$ was carbonated at 80 ℃. The formation of aragonite was favored in a suspension with a high concentration of Ca^{2+} and a minimum Mg^{2+}/Ca^{2+} molar ratio greater than 0.12. Additionally, amorphous phases including alumina-silica gel and silica gel were also detected. By mixing the AWM with cement, a new type of micro-fiber reinforced cement was developed, which showed significant mechanical performance improvement and embodied CO_2 content (25.3%).

Key words: Carbonation; Micro-fiber reinforced cement; aragonite whisker; CO_2 sequestration

1. Introduction

The world is facing a great environmental challenge due to the excessive release of CO_2. Cement is one of the most widely used man-made materials in the world and its production accounts for about 8% of global anthropogenic CO_2 emissions [1], contributing from both fuel combustion and the calcination process of limestone (calcium carbonation (CC)). Due to improvements of thermal efficiency of modern combustion system, the CO_2 resulting from the decomposition of CC accounts for about 70% of total CO_2 emission in advanced cement plants [2]. Since it is hard to further improve the thermal efficiency of mature cement plants [3]. Thus, reducing the CO_2 from the decomposition of CC would be the most viable way to mitigate CO_2 emission from cement production. Therein, the use of non-carbonate materials is already being practiced [4]. However, the reductions in energy use and absolute CO_2 emission resulting from decomposition would reach their limit in the near future [4]. Further innovations in reducing CO_2 emission of cement production is required in the area of CO_2 capture and storage technologies, which shows the potential to reach zero emission in cement production [5-9].

CO_2 capture and storage technologies can prevent CO_2 from being released into the atmosphere. Depends on the engagement stages, there are mainly four categories of CO_2 capture and storage technologies that have been investigated and proposed, including employ retrieve processes at the pre-combustion, post-combustion, oxyfuel combustion, and industrial separation stages [10]. Among these technologies, the post-

combustion process is the preferred option as it only requires slightly retrofitting existing facilities and have limited impact on the existing cement production procedures[11]. Carbon capture technologies such as chemical absorption [6, 12], membrane separation [13] and sorption with solids [14, 15] have been used to capture CO_2 from kiln-off gas. Although some of these technologies have been validated at the pilot scale, few of them has been demonstrated at commercial scale [5]. Moreover, the overall cost of cement production increased by 49-92 % for cement manufactures running carbon capture equipment compared to conventional plants [16]. Further research and development are urgently needed to make CO_2 capture and storage technologies economically viable.

In fact, Portland cement can be used as an excellent CO_2 capture and storage material to absorb CO_2 in flue gas, which possesses a high carbonation reactivity and has a carbon sequestration potential that is theoretically equal to the CO_2 emitted from the decomposition of limestone during the cement making process [17, 18]. It has potentials to absorb CO_2 in flue gases. Regarding the carbonation mechanisms of Portland cement, the calcium silicates including alite (C_3S) and belite (C_2S) have good carbonation reactivities [19]. Calcium carbonate (CC) and an amorphous alumina-silica gel are the main carbonation products [19, 20]. Generally, three main polymorphs of CC can be observed in carbonated cement [21, 22], which are calcite, aragonite and vaterite. Referring to aragonite, as a metastable CC polymorph, it usually presents a needle-like shape [23]. Also, vaterite is also unstable and these two CC polymorphs

may eventually convert to calcite [24].

Furthermore, conventional concrete is regarded as a brittle material, where cracks can be easily generated by thermal stress, shrinkage stress, and other external loadings. The addition of fiber is one of the most effective ways to improve the toughness and tensile strength of concrete [25-28]. Among various fibers, micro-fibers including carbon nano-tubes [29], carbon (including graphene) fiber [30], polyvinyl alcohol fiber [31], micro-steel fiber [32] and micron size calcium carbonate whisker [25, 33] can arrest the generation and propagation of micro-cracks, which are effective in improving tensile strength and toughness of cement-based materials [34, 35]. Needle-like aragonite whisker, a micro-fiber with a length of 10-30 μm and diameter of 0.5-3 μm is also a promising material to be used for micro-fiber reinforced cement-based materials due to its relatively low production cost [36], and ability to enhance the mechanical properties and crack resistance of concrete [25, 37-39].

As mentioned above, even though a large amount of CO_2 is released during cement production, the produced cement clinkers have a high carbonation reactivity, and upon which carbonation products with a high proportion of CC would be produced. In fact, the needle-like aragonite can be stably produced through the carbonation of cement based materials if the transformation of aragonite to calcite is inhibited. Usually, the formation and conversion of CC follows the Ostwald's process, that is, all the metastable CC polymorphs tend to be transformed to calcite, which is the most stable polymorph [40-42]. It has been reported that the conversion of CC polymorphs depends

on many factors such as relative humidity, CO_2 concentration, pH value and magnesium content etc. [43-46], and the relative amounts of different CC polymorphs formed varied in different studies. Also, certain additives can be added to control the CC crystallization during carbonation, for example, amino acids promoted the formation of amorphous CC, vaterite and aragonite [47], and an appropriate amount of chitosan promoted the aragonite formation and increased CC crystal size of the carbonated γ-C_2S [48]. Because of these complex factors, no study has reported on the relative amounts of different CC polymorphs formed in the carbonated cement based materials.

However, aragonite whiskers, as a manmade commercial product, had been produced by a carbonation process of $Ca(OH)_2$ in the presence of crystal stabilizers and precursors [49, 50]. Due to the significant amount of calcium content, it seems to be suitable to use Portland cement to prepare aragonite whiskers through carbonation process involving the presence of stabilizers and precursors. Thus, aragonite whisker-rich materials (AWM) containing needle-like whiskers and reactive amorphous gels can be produced at cement plants by using cement clinkers and flue gas. Furthermore, a new micro-fiber reinforced Portland cement can be conveniently and economically obtained by mixing the produced AWM and the original cement. The flue gas from the cement plants containing a high concentration of CO_2 that can be used as the CO_2 source to carbonate cement directly and rapidly under a wet condition [19]. Thus, this study proposed a new CO_2 capture technology that can reduce CO_2 emission efficiently and contribute to the forthcoming CO_2 neutral economy. Therefore, the systematically

investigations on carbonation process and mechanism were needed to verify the feasibility of proposing approach.

In this paper, a wet carbonation approach is reported to prepare AWM, aiming to capture CO_2 in the flue gas and prepare value-added products in the cement plant at the same time. The prepared AWM was used to produce micro-fiber reinforced cement with a low carbon footprint. Magnesium chloride was used as a crystal stabilizer to optimize the synthesized aragonite whisker [49, 50]. A gas mixture with a CO_2 concentration of 20 % (20 % pure CO_2 and 80 % N_2) was used to simulate the kiln-off gas in cement plants. The effects of magnesium chloride concentration, temperature and carbonation duration on the generation of carbonation products were investigated using powdered X-ray diffraction (XRD), Fourier transformation-infrared spectroscopy (FTIR), scanning electron microscopy (SEM) and Solid-state nuclear magnetic resonance (NMR). The carbonation mechanisms behind the formation of AWM and the CO_2 sequestration ability during the wet carbonation process were systemically explored. The mechanical properties and hydration heat of the micro-fiber reinforced cement were validated, and the benefits of CO_2 emission reduction were discussed.

2. Material and methods

2.1 Materials and preparation

2.1.1 Materials

A type I Portland cement (CEM I 52.5) produced by Green Island Cement was used in this study and its chemical compositions are shown in Table 1. The cement had

a specific density of 3.09 g/cm^3 and a BET specific area of 861.7 m^2/kg. River sand with a size less than 2.36 mm was used as the aggregate. Magnesium chloride hexahydrate ($MgCl_2 \bullet 6H_2O$) (Analytical Grade, Fluka) was used as the crystal stabilizer. Deionized (DI) water and commercially sourced gases (CO_2 and N_2) with a concentration of 99.9 % were used.

Table 1 Chemical compositions of Portland cement (wt. %)

Oxide	Na_2O	Al_2O_3	SiO_2	Fe_2O_3	SO_3	CaO	MgO	K_2O	LOI
%	0.13	7.32	19.61	3.32	2.03	63.15	2.14	0.59	1.09

2.1.2 Design and preparation of micro-fiber reinforced cement

In order to produce the micro-fiber reinforced cement, a process was designed as shown in Figure 1. Firstly, the cement powder was mixed with $MgCl_2$ solution to prepare a cement slurry suspension, then, the gas containing CO_2 was injected into the suspension to produce AWM. After a filtration process, the produced AWM was mixed with a new batch of cement to produce micro-fiber reinforced cement.

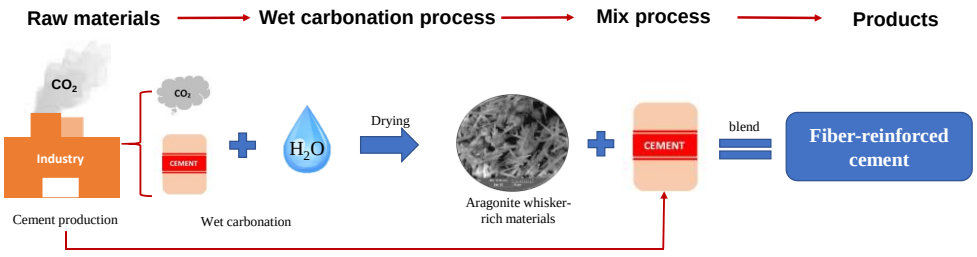

Figure 1 Design and preparation process of micro-fiber reinforced cement

In order to realize this design, an experiment program was planned to model this

industrial process in the laboratory. Commercially sourced CO_2 and N_2 were mixed to simulate flue gas emitted from cement production, and 20 % CO_2 concentration was chosen based on the CO_2 concentration of flue gas produced from the cement industry [5]. Figure 2 shows the experimental setup for the preparation of AWM.

The detailed experimental process is as follows: firstly, 15 g of cement was mixed with 300 mL of $MgCl_2$ solution thoroughly by using an electrical stirrer. The $MgCl_2$ was chosen as a crystal stabilizer due to its ability to promote aragonite nucleation [49, 50]. The concentrations of 0 M/L, 0.01 M/L, 0.025 M/L, 0.05 M/L and 0.1 M/L were considered to find an optimal one; Secondly, mixed gas containing 20 % CO_2 was injected into the aqueous system with a flow rate of 1 L/min at given temperature to control the crystal structure of CC. The suspension was mechanically stirred at a speed of 300 rpm. Different temperatures including 20 ℃, 40 ℃, 60 ℃ and 80 ℃ were evaluated to obtain an optimal temperature in this study. Also, the carbonation durations of 30 min, 60 min, 120 min and 240 min were investigated; Thirdly, after carbonation, the suspended solid was collected by a filtration process using filter funnel and filter paper (2.5 μm), and then dried in a freeze dryer. Finally, the dried solid with was mixed with a new batch of cement using dosage ratios of 5 %, 10 % and 20 % to prepare micro-fiber reinforced cement.

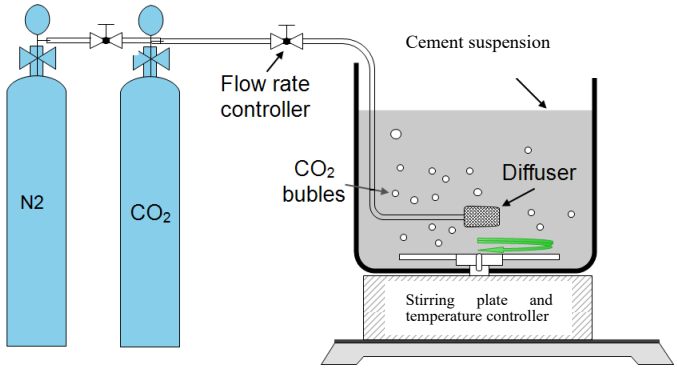

Figure 2 Illustration of setup for the preparation of AWM in the laboratory

2.1.3 Mixture proportion of micro-fiber reinforced cement mortar

Mortar samples with a water to cement ratio of 0.45 and sand to cement ratio of 2.5 were prepared to evaluate the mechanical properties of the micro-fiber reinforced cement.

2.2 Test methods

2.2.1 X-ray Powder Diffraction (XRD)

A X-ray diffractometer (Rigaku Smart-Lab) equipment Cu-Kα radiation (λ=1.54 Å) was used to measure the XRD spectra of carbonated cement. A range of 5-70 ° was chosen, and it was conducted with a scan speed of 5 °/min and a step of 0.02 °. The Rietveld analysis of the sample incorporating with 10 wt.% corundum was performed by using a TOPAS 5.0 software. 10 wt.% corundum was added into the samples as a benchmark to quantitatively determine the content of non-crystalline phases. The Inorganic Crystal Structure Database (ICSD) was used for Rietveld refinement and calculation. The contents of different phases could be obtained by peak functions based

on the XRD results and the crystal structures of the phases. The refined parameters such as zero-shift error, background coefficients, cell parameters, peak shape parameters etc. were optimized. Meanwhile, the Lorentz polarization factor was fixed to be zero and the peak shape was fitted based on the FP peak function. The weighted profile R-factor (R_{wp}) value was below 10%, which ensured the satisfactory fit quality and good Rietveld refinement results.

2.2.2 Fourier transformation-infrared spectroscopy (FTIR)

The FTIR spectra of samples carbonated with different conditions was tested by an FTIR Spectrometer (PerkinElmer UATR Two). A range of 4000-500 cm^{-1} with a resolution of 1 cm^{-1} was chosen for all the tests. An averaging 64 scans for each measurement was conducted. Before test, all the samples were dried in a drying oven.

2.2.3 Scanning electron microscopy (SEM)

The SEM images of the carbonated cement were captured by using a scanning electron microscope (Tescan VEGA 3 apparatus) with an accelerating voltage of 20 kV. The powder samples collected from carbonation were coated on carbon conductive tape. The prepared powder was stuck on a conducting resin and coated with gold before the test.

2.2.4 Thermal analysis (TGA)

The thermalgravimetric analysis (TGA) of the carbonated cement was performed to represent the composition of carbonation products. A heating range of 40 ℃ to 1000 ℃ was set, and all the tests were performed with a heating rate of 10 ℃/min under N_2 striping gas with a thermogravimetry analyzer (Rigaku, Thermo plus EVO2). Before

the test, the powder samples were dried in a vacuum oven for 24 h.

2.2.5 Solid-state Nuclear Magnetic Resonance (NMR)

The ^{27}Al and ^{29}Si MAS NMR spectra of the samples carbonated at different times (0 min, 30 min, 60 min, 120 min and 240 min) were acquired to evaluate the changes of the alumina and silica-bearing phases. A solid-state NMR spectrometer (JEOL ECZ500R) was used. The ^{29}Si NMR spectra were tested with a spinning speed of 4 kHz and a relaxation delay of 20 s by using a 7 mm triple-resonance probe, and the ^{27}Al spectra were obtained by using a 3.2 mm triple-resonance probe with a spinning speed of 12.5 kHz. Before the test, the powder samples were dried in a vacuum oven for 24 h.

2.2.6 Inductively coupled plasma-optical emission spectrometer (ICP-OES)

The concentrations of Ca^{2+} and Mg^{2+} in the cement-$MgCl_2$ suspension were tested before and during carbonation process. The inductively coupled plasma-optical emission spectrometry (ICP-OES, Spectro Blue) was used for the analysis. The filtrates of the samples were collected at 2 min and 5 min before injecting CO_2, also at 5 min, 10 min, 15 min, 20 min, 30 min and 60 min after injecting CO_2. Before the ICP test, the filtrates were digested by concentrated nitric acid [51].

2.2.7 Mechanical properties

A mortar with a water to binder ratio of 0.45 and sand to binder ratio of 2.5 was prepared for mechanical properties measurement. Prism samples with the size of 40

mm × 40 mm × 160 mm was cast. After water curing for 3 d, 7 d and 28 d, the equivalent compressive strength and flexural strength tests were conducted using a loading rate of 0.6 MPa/s and loading rate of 50 N/s, respectively.

2.2.8 Hydration heat

The hydration heat of micro-fiber reinforced cement containing different amount of AWM (0 wt.%, 5 wt.%, 10 wt.% and 20 wt.%) was tested by an isothermal calorimeter (I-Cal 4000, Calmetrix). The samples of 50 g powders and mixed with 20 g DI water. The heat flow and cumulative heat were collected under a constant temperature of 20 ℃ for 72 h.

2.2.9 BET surface area

The BET surface area of prepared AWM was determined by using a BET surface area and porosimetry system (Micromeritics ASAP 2020). The BET surface area of the samples could be acquired from the desorption isotherms

3. Results and analysis

3.1 Effect of magnesium chloride concentration on the carbonation products

3.1.1 Composition evolution of carbonation products

The effect of $MgCl_2$ concentration on the phase assemblage of cement after carbonating for 60 min was determined by XRD (Figure 3) and FTIR (Figure 4). The detailed contents of aragonite, calcite and clinker phases (revealed by Rietveld analysis) are shown in Table 2.

The XRD spectra of the samples prepared with different concentrations of $MgCl_2$ solution are shown in Figure 3. As well known, the main clinker compositions of OPC are C_3S, C_2S, C_3A and C_4AF. For all the samples carbonated in $MgCl_2$ solutions with different concentrations, the amounts of clinker phases were significantly reduced, while newly formed CC became the dominant crystalline component. The $MgCl_2$ concentration had noticeable effects on the carbonation rate and carbonation products formed. Firstly, the residual amount of clinker phases increased with the increasing $MgCl_2$ concentration, while the amount of crystalline CC content decreased. Secondly, aragonite started to be present after $MgCl_2$ was added, becoming the dominant polymorph of CC when the $MgCl_2$ concentration reached 0.025 M/L. However, 0.1 M/L $MgCl_2$ concentration is not recommended, as the aragonite content was decreased along the further increase of the $MgCl_2$ concentration. To be more specific, the calcite content decreased from 71.27 % to 5.76 % as the $MgCl_2$ concentration was increased from 0 M/L to 0.05 M/L. At the same time, the aragonite content increased from 1.59 % to 60.87 %. However, the aragonite content was reduced to 47.49 % when the $MgCl_2$ concentration was further increased to 0.1 M/L. It should be noted that the total amount of CC decreased when the $MgCl_2$ was added, indicating a reduced carbonation degree.

Overall, the $MgCl_2$ not only decelerated the carbonation rate of cement but also promoted the transformation from calcite to aragonite. The presence of $MgCl_2$ did not influence the carbonation of C_4AF, which might be attributed to the low carbonation reactivity [52]. Based on the results, a $MgCl_2$ concentration higher than 0.025 M/L

should be chosen to prevent the transformation from aragonite to calcite completely.

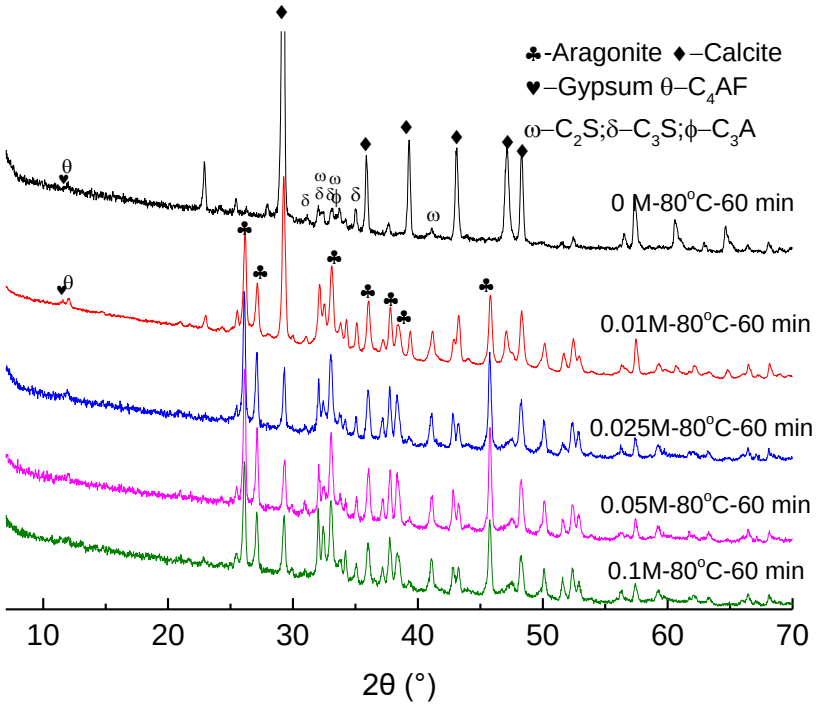

Figure 3 XRD spectra of cement carbonated with different concentration of $MgCl_2$

Table 2 Amounts of carbonation products obtained by Rietveld analysis (wt.%)

NO.	C_3S	C_2S	C_4AF	C_3A	Calcite	Aragonite	Gypsum	ACn
0M-80°C-60min	2.81	0.92	6.02	2.02	71.27	1.59	0.77	14.60
0.01M-80°C-60min	8.76	4.70	6.13	3.48	21.63	40.09	0.07	15.14
0.025M-80°C-60min	7.73	5.60	5.37	5.21	5.41	61.00	1.04	8.63
0.05M-80°C-60min	6.86	4.63	5.72	4.97	5.76	60.87	0.76	10.44
0.1M-80°C-60min	11.68	7.24	6.52	6.00	5.02	47.49	0.49	15.56

Note: ACn is the amorphous and crystalline non-quantified (ACn) content

Figure 4 shows the FTIR spectra of the samples prepared with different concentrations of $MgCl_2$. Usually, the asymmetric stretch of the carbonate ions at 1488 cm^{-1} accompanied with the absorption peak at 699 cm^{-1} was the characteristic of amorphous calcium carbonate (ACC) [53, 54]. Compared to the samples carbonated in DI water, the involvement of $MgCl_2$ leaded to a distinct absorption peak at 699 cm^{-1}. In

addition, the broad absorptions peaks between 900 cm^{-1} and 1200 cm^{-1} [55] related to the vibration of Si-O bonds also changed with the variation $MgCl_2$ concentration, specially, the absorption peaks became narrower with the increase of $MgCl_2$ concentration, suggesting the reduced decalcification degree of calcium silicate. Also, the peak shifted from 1038 cm^{-1} to 1010 cm^{-1} as the $MgCl_2$ concentration was increased from 0 M/L to 0.1 M/L, indicating the reduced polymerization of Si [56]. The absorption bands located at about 1416-1470 cm^{-1} and 853-873 cm^{-1} could be assigned to the symmetric stretch and out-of-plane bending bands of the C-O bond. These absorption bands located at about 1400-1490 cm^{-1} shifted to higher values while the absorption at 850-880 cm^{-1} shifted to a lower value after adding $MgCl_2$, which might reflect the transformation from calcite to aragonite. Therefore, the increased $MgCl_2$ concentration not only rendered the preferential formation of aragonite but also promoted the generation of ACC due to the stabilization effect of magnesium [57, 58]. A $MgCl_2$ concentration higher than 0.025 M/L but lower than 0.1 M/L would be chosen to ensure a high aragonite content and reduced the ACC formation based on the XRD and FTIR results.

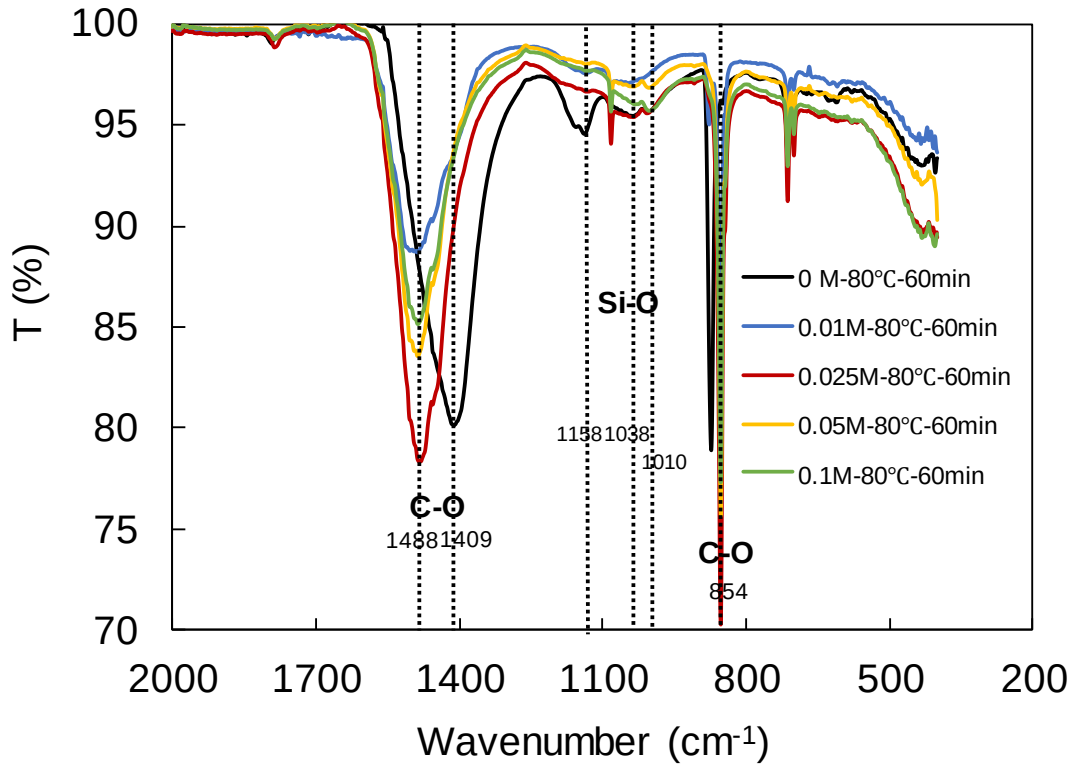

Figure 4 FTIR spectra curves of cement carbonated with different concentrations of $MgCl_2$ solution

3.1.2 Microstructure

The morphologies of the cement carbonated for 60 min at different concentrations of $MgCl_2$ solution are shown in Figure 5. It can be observed that the morphology of carbonated products was strongly associated with the $MgCl_2$ concentration. For the cement carbonated in DI water, aggregated grains with a rhombohedral shape grew on the surface of cement particles. However, the morphology was significantly changed for the cement carbonated in $MgCl_2$ solution with a concentration of 0.01 M/L. Needle-like aragonite with a small diameter and rhombohedral-shaped calcite were both present. Interestingly, calcite could not be observed when the $MgCl_2$ concentration was higher than 0.025 M/L, indicating the new-formed aragonite was dominant in the reaction

products while the formation of calcite was hindered completely. This was in agreement with the QXRD results. The morphology of aragonite was also closely related to the $MgCl_2$ concentration. These thin aragonite crystals grew bigger with the increase of $MgCl_2$ concentration, and a needle-like crystal structure was obtained at 0.05 M/L where a single crystalline particle measured a length of 10-30 μm and diameter of 0.5-2 μm grew on the surface of cement. These aragonite whiskers connected with each other and grew on the un-carbonated cement core. This evidence that the presence of $MgCl_2$ strongly promoted the formation of this mineral. Also, aggregated cottony materials located between the aggregated aragonites could be observed in the samples carbonated in the $MgCl_2$ solution. Based on the XRD and SEM results, a $MgCl_2$ concentration of 0.05 M/L was therefore chosen to ensure the formation of aragonite with a needle-like morphology.

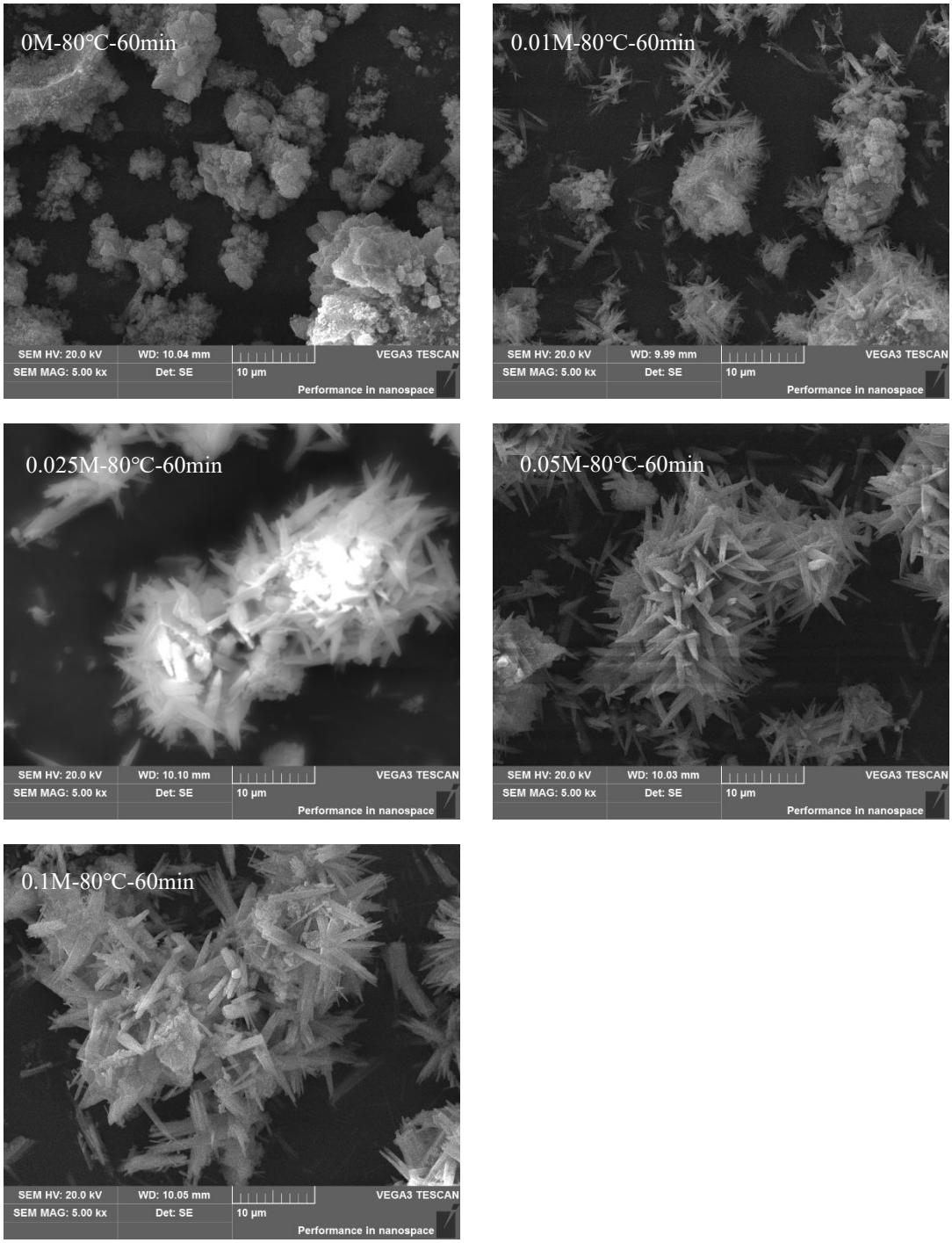

Figure 5 Morphology of cement carbonated in different concentrations of $MgCl_2$

3.2 Effect of temperature on the carbonation products

3.2.1 Composition evolution of carbonation products

The effect of temperature on the carbonation products of the sample carbonated for 60 min was also characterized by XRD (Figure 6) and FTIR (Figure 7). The contents

of aragonite, calcite and clinker phases have been revealed by Rietveld analysis and are shown in Table 3.

Figure 6 shows the XRD spectra of the samples carbonated in 0.05 M/L $MgCl_2$ solution at different temperatures. The XRD spectra shows that the polymorphs of CC and their contents were strongly associated with the carbonation temperature. In general, almost all the CC was calcite in the sample carbonated at 20 ℃, while the calcite started to transform to aragonite at 40 ℃. As a result, the calcite content decreased from 49.08 % to 5.76 % as the temperature was increased from 20 ℃ to 80 ℃, but the aragonite content increased from 0 % to 60.87 % at the same time. The aragonite became the main polymorph of CC at 60 ℃. In addition, the total amount of crystalline CC was first decreased to 44.87 % at 40 ℃ and then increased with the further increase of temperature. Meanwhile, the amounts of residue clinker phases including C_2S, C_3S and C_4AF showed an opposite trend. Therefore, the carbonation temperature was another key factor controlling the formation of CC polymorphs and the carbonation rate. In order to prepare AWM by carbonating cement, a carbonation temperature higher than 60 ℃ and $MgCl_2$ solution with a concentration of 0.05 M/L were required.

Table 3 Contents of carbonation products obtained by Rietveld analysis (wt.%)

NO.	C_3S	C_2S	C_4AF	C_3A	Calcite	Aragonite	Gypsum	ACn
0.05M-20°C-60min	14.23	10.90	7.50	7.93	49.08	0.00	0.67	9.69
0.05M-40°C-60min	14.51	8.47	5.99	7.44	26.16	18.71	0.69	18.03
0.05M-60°C-60min	5.21	6.34	6.64	4.80	5.56	53.69	0.54	17.21
0.05M-80°C-60min	6.86	4.63	5.72	4.97	5.76	60.87	0.76	10.44

Note: ACn is the amorphous and crystalline non-quantified (ACn) content

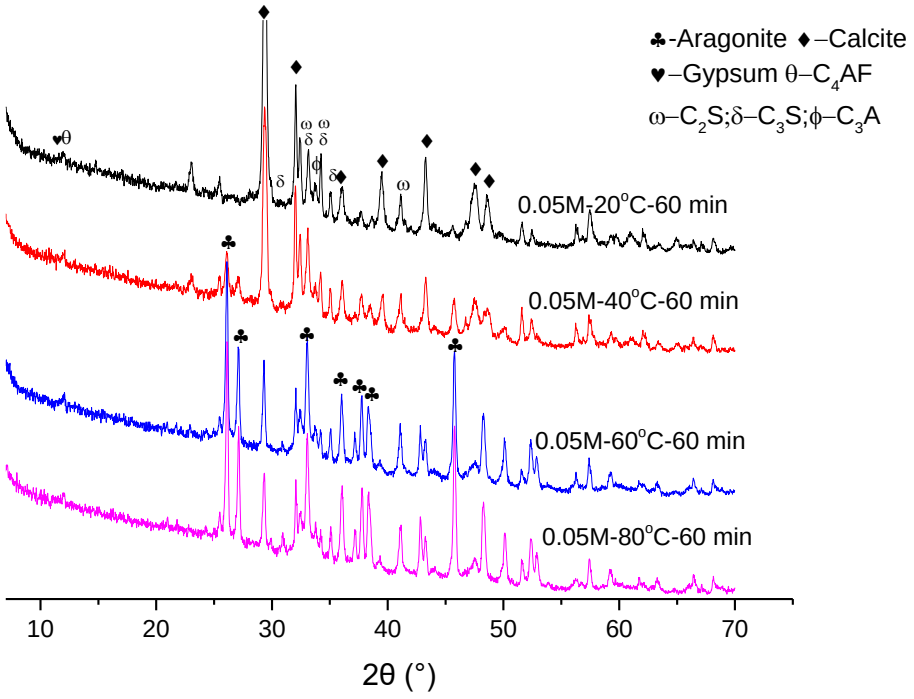

Figure 6 XRD spectra of samples carbonated in 0.05M solution at different temperature

Figure 7 shows the FTIR spectra of the samples carbonated for 60 min at 20 ℃, 40 ℃, 60 ℃ and 80 ℃, respectively. The spectra indicated that the absorption peaks associated with the vibration of Si-O bond [55, 59] were influenced by the carbonation temperature. The narrower peak and lower intensity of samples carbonated at higher temperature, indicating a reduced polymerization of the silica-bearing materials [56]. The vibration of C-O bond was also observed, which could be used to characterize the formation of CC. Also, the presence of ACC was confirmed in the samples carbonated at 60 ℃ and 80 ℃ due to the appearance of the asymmetric stretch of the carbonate ions at 1488 cm^{-1} accompanied by the absorption peak at 699 cm^{-1} [53, 54]. Therefore, the increased temperature reduced the polymerization of the newly formed silica-bearing materials and promoted the formation of ACC.

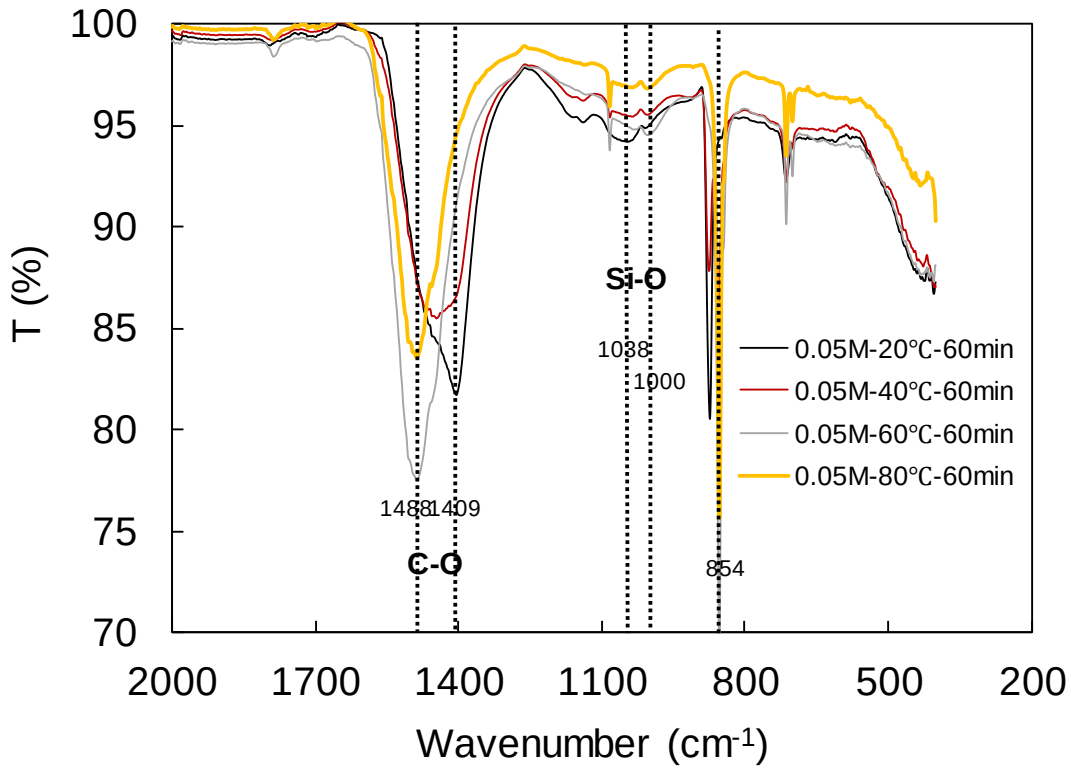

Figure 7 FTIR spectra of samples carbonated at 20 ℃, 40 ℃, 60 ℃ and 80 ℃

3.2.2 Microstructure

Figure 8 shows the morphologies of the cement carbonated at 20 ℃, 40 ℃, 60 ℃ and 80 ℃. The carbonation temperature had a significant influence on the microstructure of the carbonated samples. The rhombohedral-shaped calcite without clear edges grew on the cement particles at 20 ℃. For the samples carbonated at 40 ℃, both clusters of different-oriented aragonite and rhombohedral-shaped calcite were present. For the samples carbonated at 60 ℃, the rhombohedral-shaped calcite was fully replaced by the clusters of different-oriented aragonite. Moreover, the aragonite turned to the needle-like shape at 80 ℃. Therefore, the increased temperature not only promoted the aragonite formation but also affected its morphology. In order to prepare

needle-like aragonite whiskers, a temperature higher than 80 ℃ should be used.

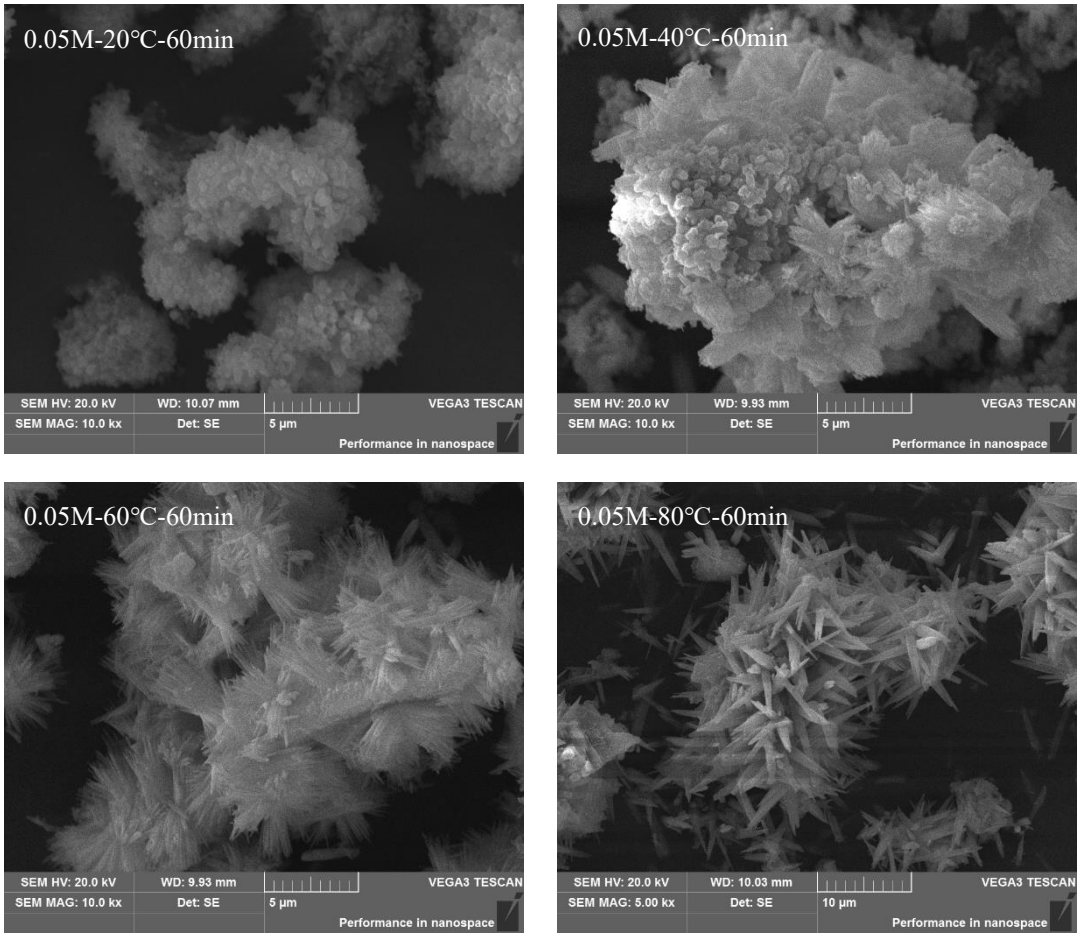

Figure 8 The morphologies of samples carbonated at 20 ℃, 40 ℃, 60 ℃ and 80 ℃

3.3 Effect of carbonation duration

3.3.1 Evolution of carbonation phases

Based on the results in sections 3.1 and 3.2, the optimized carbonation conditions for aragonite formation with a $MgCl_2$ concentration of 0.05 M/L and a temperature of 80 ℃ were selected. In order to better understand the mechanism of the aragonite formation, the evolution of carbonation phases was further characterized by QXRD (Figure 9), TG (Figure 10), FTIR (Figure 11), ^{29}Si NMR (Figure 12) and ^{27}Al NMR

(Figure 13) methods. The quantitative mineral composition of cement and crystalline carbonation products is shown in Table 4.

(1) Evolution of calcium phases

The XRD spectra of the samples carbonated for 0 min, 30 min, 60 min, 120 min and 240 min are shown in Figure 9. The Rietveld analysis was used to obtain the contents of the carbonation products and residual cement phases (shown in Table 4). The XRD spectra of the reference sample revealed that the main components of cement were C_3S, C_2S, C_4AF, C_3A, calcite and gypsum. After mixing with $MgCl_2$ solution, brucite was quickly formed before CO_2 injection. Afterwards, the amount of aragonite increased rapidly and the content of clinker phases decreased with increasing carbonation time. It should be noted that brucite disappeared at about 30 min of carbonation.

Generally, the amount of aragonite increased from 0 % to 68.53 % as the carbonation time was increased from 0 min to 240 min. The calcium silicates including C_3S and C_2S were nearly exhausted at 240 min, but about 3.27 % C_3A and 4.96 % C_4AF were still remained. Among these four principal clinkers, C_3S showed the highest carbonation reactivity. About 74.38 % C_3S had already been consumed after 30 min, but further reaction was slower and the total carbonation degree was 97.10 % after carbonating for 240 min. C_2S had the second fast carbonation reactivity, and the carbonation degree reached 58.77 % at 30 min and 98.05 % at 240 min. Compared with the calcium silicates, the carbonation rates of C_3A and C_4AF were slower, where

reactions degrees of 54.06 % and 70.27 % were recorded respectively at 240 min. The difference in carbonation rates of these four clinker phases might be linked to the different dissolution rates of Ca^{2+} [60].

Table 4 Amounts of carbonation products obtained by QXRD (Rietveld analysis) (wt.%)

NO.	C_3S	C_2S	C_4AF	C_3A	Calcite	Aragonite	Gypsum	ACn
0.05M-80°C-0min	48.57	21.34	9.71	9.89	5.75	0.10	2.37	0.47
0.05M-80°C-30min	13.82	10.60	7.43	5.72	6.43	51.72	0.79	3.47
0.05M-80°C-60min	6.86	4.63	5.72	4.97	5.76	60.87	0.76	10.44
0.05M-80°C-120min	3.54	1.94	5.33	3.47	4.42	62.47	0.37	18.47
0.05M-80°C-240min	1.57	0.50	4.96	3.27	5.36	68.53	0.78	15.04

Note: ACn is the amorphous and crystalline non-quantified (ACn) content

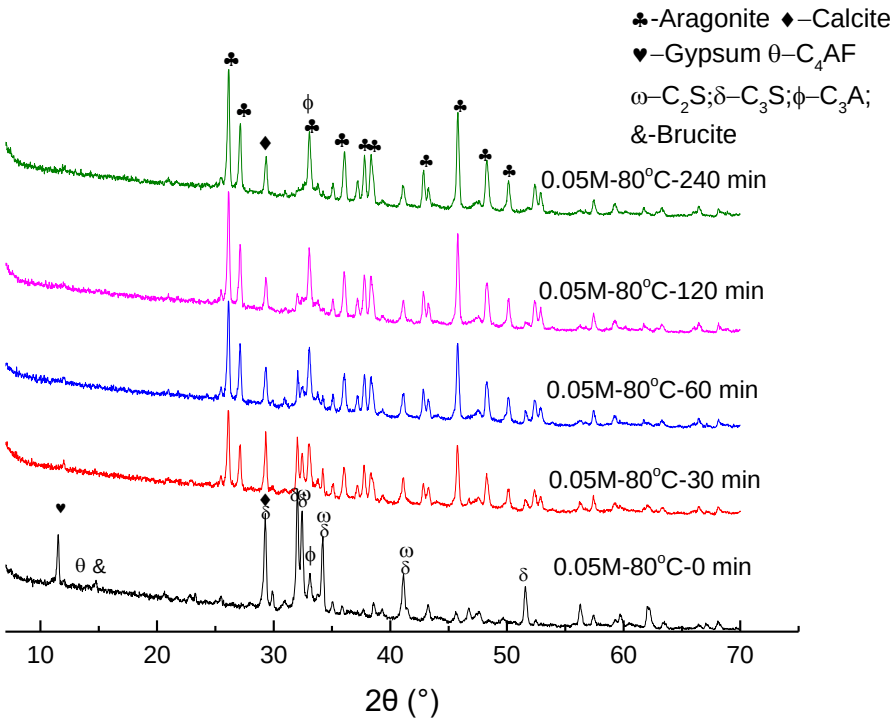

Figure 9 XRD spectra of samples carbonated for different times

Thermal analysis was also conducted to reveal the carbonation products (shown in

Figure 10). For the samples without carbonation, the presence of brucite was confirmed from the peak located at about 400 ℃ [61, 62]. But brucite disappeared after injecting CO_2, and a small peak located at about 470 ℃ was observed. This new peak can be attributed to the decomposition of the residual magnesium chloride hexahydrate (MCH) [63]. The CC comprising calcite and aragonite [49, 64, 65] could be revealed by the peak at about 670-740 ℃. Similar to the XRD results, CC formed rapidly after injecting CO_2, and its amount increased quickly within 30 min and leveled off afterwards and reached a total content more than 60 % after 240 min. Interestingly, according to the DTG curves, the center of peaks associated with the decomposition of CC was shifted. Specifically, it was increased from 680 ℃ to 730 ℃ as the $MgCl_2$ concentration was increased from 0 M/L to 0.1 M/L. The increased temperature was attributed to the formation of polymorphs of CC, especially aragonite has a higher decomposition temperature than that of calcite [66].

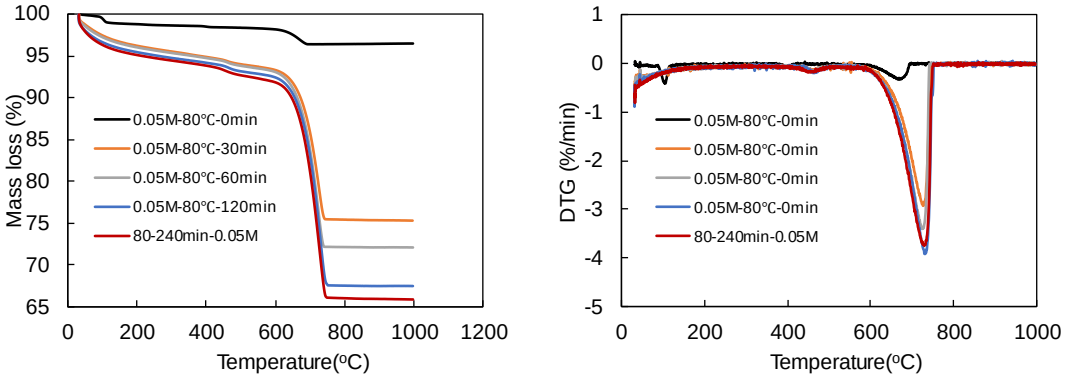

(a) TG (b) DTG

Figure 10 Thermal analysis of samples carbonated for different times

The FTIR spectra of the samples carbonated for different times are shown in

Figure 11. The presence of ACC was confirmed in the carbonated samples [53, 54]. The increased intensity of the absorption peak at 699 cm^{-1} revealed the increased amount of ACC. However, the amount of ACC was small and was difficult to quantify. Also, the absorptions between 900 cm^{-1} and 1200 cm^{-1} corresponding to the vibration v_3 of Si-O bond [55] became broader as the carbonation reaction progressed . These peaks at about 1038 cm^{-1} is linked with the vibration of Si-O bonds in Q^3 and Q^4, confirming the formation of silica gel [67]. The presence of absorption bands at about 1488 cm^{-1} and 854 cm^{-1} were related to the symmetric stretch and out-of-plane bending bands of the C-O bond in aragonite [54]. These absorption bands located at about 1400-1490 cm^{-1} shifted to a higher value of 1488 cm^{-1} while the absorption at 850-880 cm^{-1} shifted to a lower value of 854 cm^{-1} when the aragonite was formed, which was attributed to the polymorphs of CC.

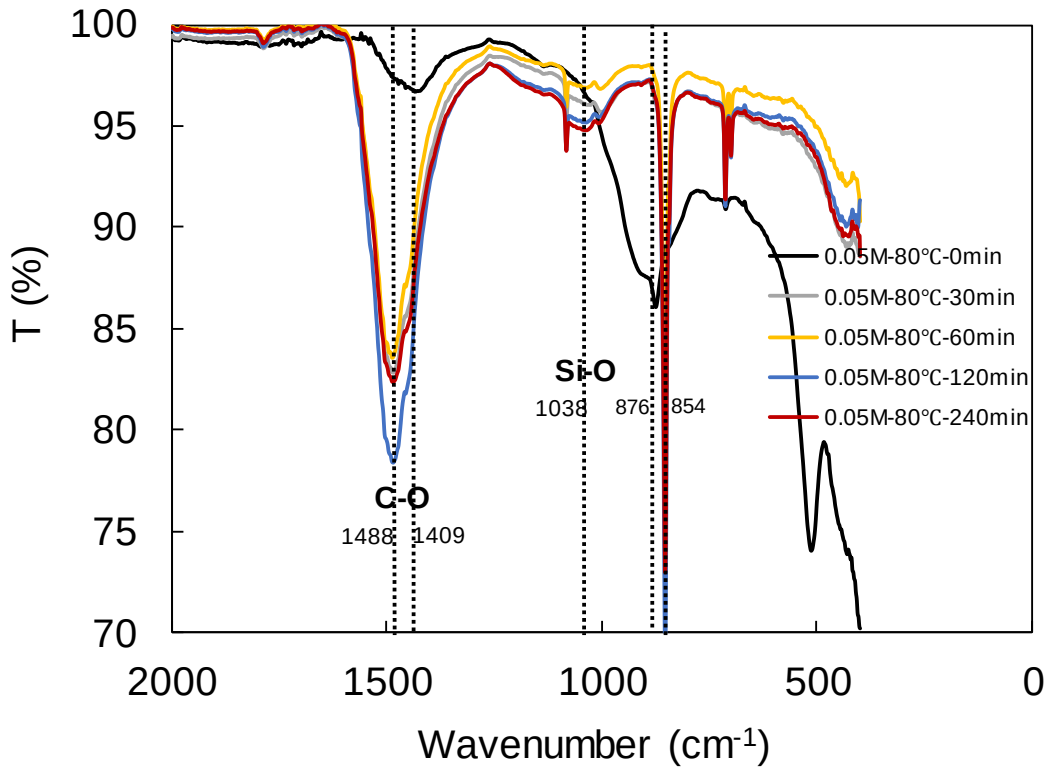

Figure 11 The development of FTIR spectra of RCF during carbonation

3.3.2 **Evolution of silica and alumina phases in carbonated cement**

The ^{29}Si NMR and ^{27}Al NMR spectra of the samples were obtained to indicate the evolution of the silica phase and the alumina phase. The ^{29}Si NMR spectra of the cement carbonated for different carbonation time are shown in Figure 12, which were labelled according to Q^n. Generally, the presence of Q^0 signal (at about -71 ppm) refers to individual silicon-oxygen tetrahedral of silicate in the clinker, Q^3 (at about -100 ppm) belongs to the hydroxylated surface sites ($(SiO)_3$–Si-OH) in the silica gel and Q^4 signal (at about -110 ppm) belongs to Q^4 ($(SiO\text{-})_4Si$) in the silica gel [68-70]. Also, a Q^{3b} signal located at about -93.4 ppm was observed which represented the presence of alumina-silica gel formed by carbonation [69]. As the cement was carbonated directly without hydration, no Q^1 site (at about -80 ppm) and Q^2 (at about -85 ppm) site associated with

C-S-H gel [71] were observed. However, the intensity of Q^0 site decreased rapidly with the increasing carbonation time, while the intensities of Q^3 and Q^4 increased. This indicated the transformation between an individual silicon-oxygen tetrahedral and a highly polymerized SiO_4 tetrahedra. It should be noted that the intensity of Q^0 decreased rapidly during the first 60 min, and after that, the carbonation of the clinker phases was slowed down. Correspondingly, Q^3 and Q^4 increased rapidly within 60 min, and their intensities increased continually between 60 min and 240 min. It worth noting that the Q^0 site was still present at 240 min.

The evolution of alumina phases was determined by ^{27}Al NMR spectra and are shown in Figure 13. For the sample without carbonation, the broad resonance centered at about 10 ppm could be observed, which is attributed to the presence of six-fold coordination in C_3A and C_4AF [69, 72]. A significant reduction of intensity of this resonance was observed within the first 30 min, indicating the rapid carbonation of C_3A and C_4AF. This was in agreement with the XRD results elaborated in previous section. A new resonance centered at about 56 ppm appeared and its intensity increased with increasing carbonation time, which indicated the increased tetrahedrally coordinated aluminum, indicating the aluminum incorporated in the alumina-silica gel [73, 74]. Similar to the silicon phase, rapid change was observed during the first 60 min. Also, a broad resonance centered at about 86 ppm was observed in the reference sample, which was associated with aluminum guest-ions incorporated in C_3S and C_2S [19]. This aluminum dissolved into solution rapidly during the carbonation of calcium silicate and

participated as an alumina-silica gel, leading to the reduced intensity of this resonance.

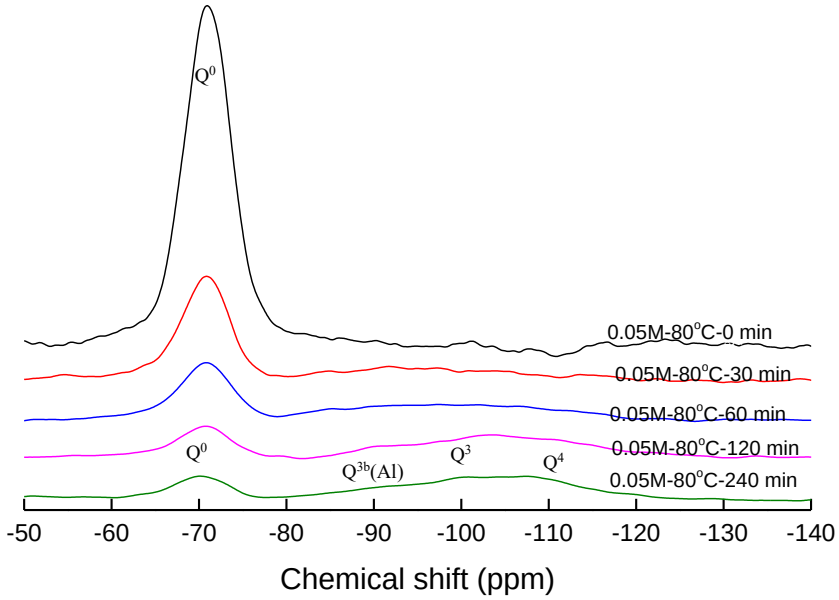

Figure 12 [29] Si NMR spectra of cement with different carbonation time

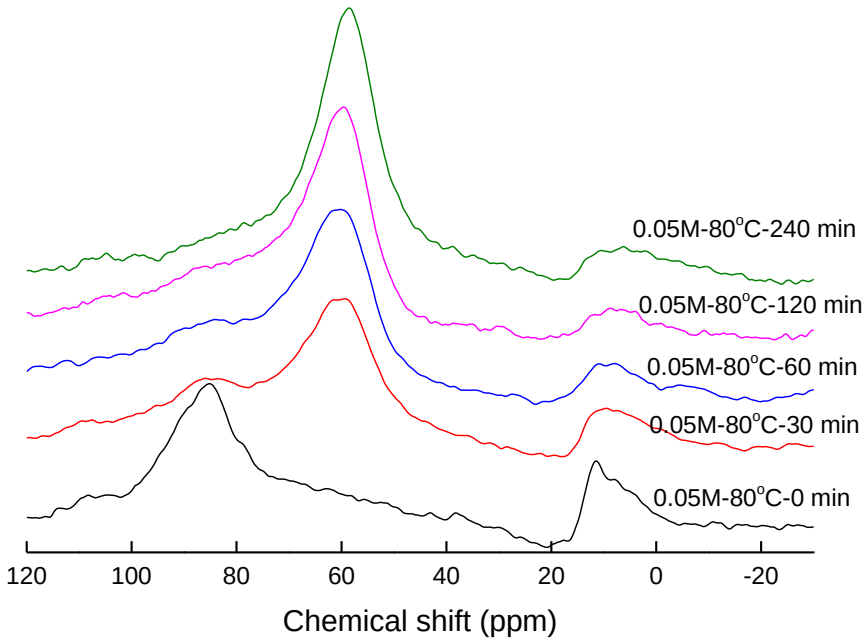

Figure 13 [27]Al NMR spectra of cement with different carbonation time

3.3.3 Evolution of microstructure

The morphology development of the samples is revealed in Figure 14. It can be

observed that dumbbell-shaped aragonite with a low length/diameter ratio and large diameter was quickly formed on the cement grains at 30 min of carbonation. Some poorly crystalline products with lumpy shapes could be observed on the grains as well. The shape of aragonite was changed with increasing carbonation time. The length/diameter ratio of the aragonite crystal increased, and it became typical needle-like at 60 min. Furthermore, needle-like aragonite with a length of 10-30 μm and a diameter of 0.5-2 μm was observed at 120 min. From the morphology development, aragonite was formed immediately after injecting CO_2. The crystal formed had an elongated shape and face-capped diameter. Some fibroid and lumpy-shaped products between the individual aragonite crystals were observed, which might be attributed to the formation of amorphous phases.

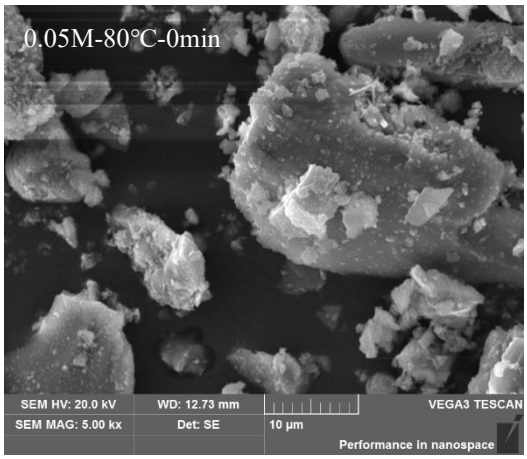

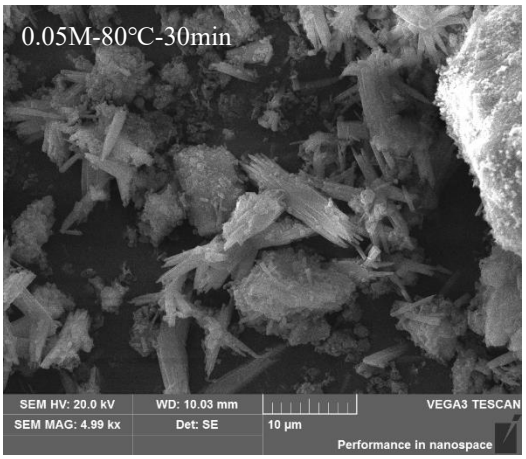

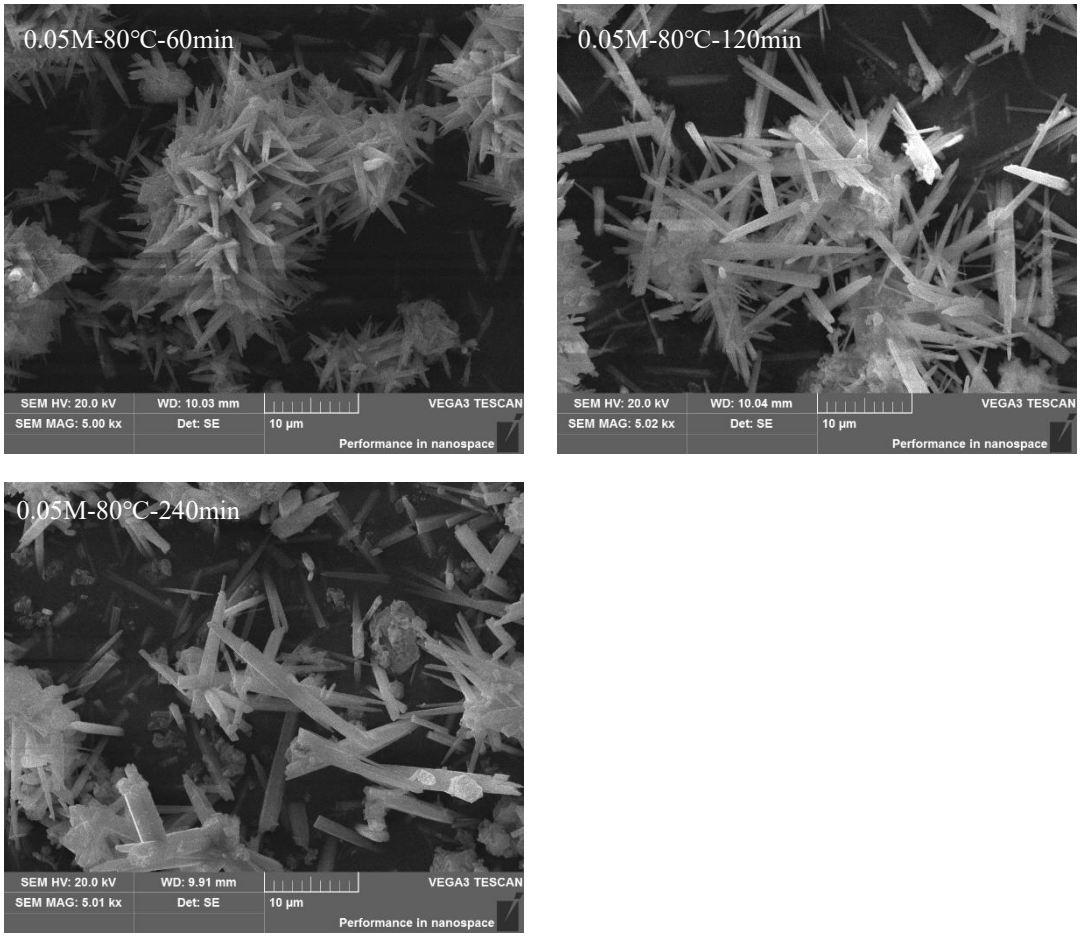

Figure 14 Morphologies of samples carbonated at different times

4. Validation of micro-fiber reinforced cement

4.1 The characteristic of prepared AWM

The particle characteristics of cement and AWM were determined using laser granulometry and BET methods, and the test results are shown in Figure 15. It can be observed from Figure 15 (a) that the particle size increased after carbonation, the amount of particle with size <10 µm was significantly reduced, and the center of the peak shifted from about 20 µm to about 30 µm. The D50 was increased from 17.69 µm to 31.46 µm corresponding to the D50 of cement and AMW (carbonated for 120 min),

respectively. In addition, from the two isotherms, the BET surface areas of cement and AWM were 1.70 m²/g and 23.45 m²/g, indicting a significant increased adsorption capacity. This might be attributed to the amorphous phases in AWM. Therefore, the prepared AWM possessed both coarsened particle size and higher BET surface area than that of cement.

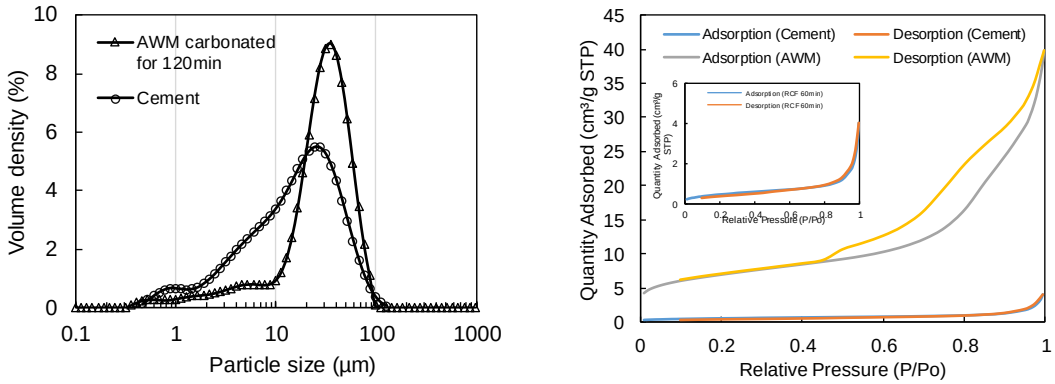

(a) Particle size distribution

(b) BET adsorption and desorption isotherm

Figure 15 The particle size distribution and BET adsorption & desorption isotherm of AWM

4.2 Hydration heat of micro-fiber reinforced cement

In order to investigate the effect of AWM on the hydration and performance of cement, the mechanical properties and hydration heat of micro-fiber reinforced cement containing different amounts of AWM (5 wt.%, 10 wt.% and 20 wt.%,) were determined.

Figure 16 shows the heat flow and cumulative heat release of the micro-fiber reinforced cement paste prepared with a water to binder ratio of 0.4. For the samples incorporated AWM, the hydration heat curves were significantly changed compared to the reference batch. Firstly, the induction period was shortened with the increase of

AWM addition. Secondly, the magnitude of main hydration heat peak related to the hydration of C_3S was increased, and a higher hydration rate was observed with the increased dosage. Thirdly, similar second peak associated with the depletion of gypsum and hydration of aluminate phases were observed.

Due to the increased heat flow rate, an improved cumulative heat release of the micro-fiber reinforced cement pastes could be observed. The cumulative heat of the micro-fiber reinforced cement paste (20 wt. % AWM) reached 217.04 J/g at 72 h, which was much higher than that of the reference cement paste (150.82 J/g). Therefore, the AWM addition led to an accelerated hydration rate and higher hydration degree. This might be attributed to the presence of the amorphous phases in the AWM, which had a very high surface area (shown in Figure 15), serving as nucleation sites that can accelerate cement hydration. Also, the amorphous phases had a very high pozzolanic reactivity [75] that consumed Ca^{2+} in the pore solution, which further promoted and accelerated the cement hydration. Furthermore, the aragonite phase in the AWM had some acceleration effect on cement hydration due to nucleation effect [76], as shown in Figure 16.

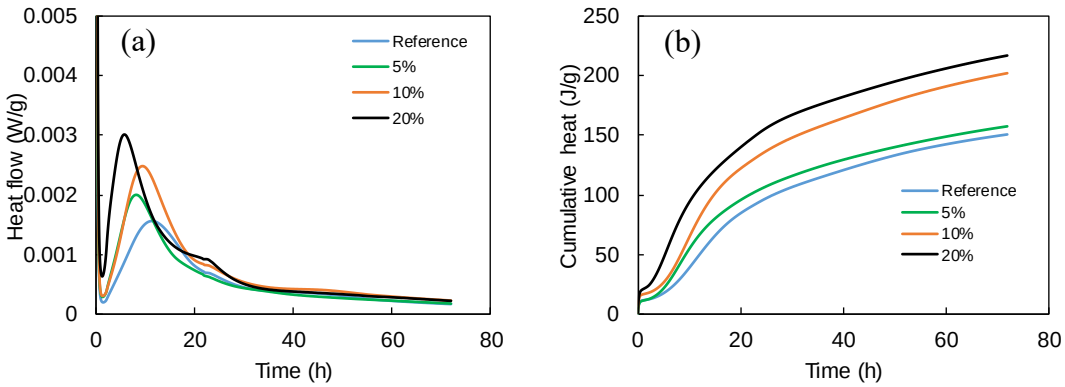

Figure 16 Influence of AWM on the hydration heat flow (a) and cumulative heat (b) of cement pastes

4.3 Evaluation of mechanical properties

Figure 17 shows the compressive strength and flexural strength of the prepared micro-fiber reinforced cement mortar containing different amounts of AWM carbonated for 120 min. It can be observed that the mechanical properties were dependent on the proportion of AWM. Both compressive strength and flexural strength were improved after adding AWM at all testing ages. For the compressive strength, the 28 d-strength of the samples incorporated with 10 % AWM reached the maximum value of 61.7 MPa, which was an increase of 24.1 % compared to that of the reference samples. But the improvement of compressive strength was reduced when the addition of AWM reached 20 % due probably to the dilution of cement content and the introduction of interface defects [33] when excess of AWM was added. The changes of flexural strength also showed a similar trend, where a maximum strength increase of 25.9 % was observed for the sample containing 5 % AWM. The improved mechanical properties can be explained by the presence of the aragonite whiskers and amorphous gels with high

pozzolanic reactivity [37, 77, 78]. Therefore, an AWM reinforced cement with excellent performance could be developed by adding AWM prepared by a sustainable wet carbonation method proposed in this study.

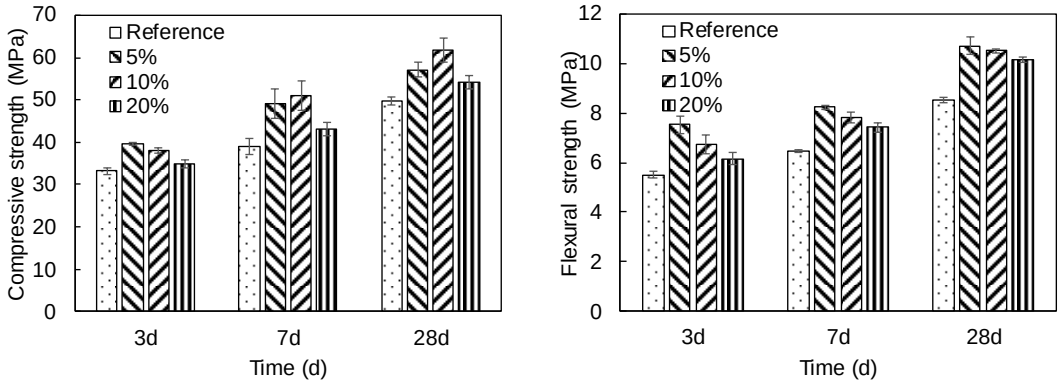

(a) Compressive strength (b) Flexural strength

Figure 17 Compressive strength and flexural strength of AWM reinforced cement mortar

5. Discussion

5.1 Phase assemblance evolution of aragonite whisker-rich materials

Based on above results, AWM could be prepared by injecting CO_2 into a hot cement suspension solution containing $MgCl_2$. The optimal temperature and $MgCl_2$ concentration were 80 ℃ and 0.05 M/L, respectively. The phases evolution and factors controlling the aragonite formation were discussed as follows:

5.1.1 Phases evolution during wet carbonation of cement

A suspension of cement-$MgCl_2$-$Mg(OH)_2$-$CaCl_2$ was immediately formed after mixing. After injecting CO_2, the Ca^{2+} dissolved from the cement clinker would react with CO_2 in $MgCl_2$ solution, resulting in the formation of aragonite, calcite or ACC.

When the $MgCl_2$ concentration was low (lower than 0.025 M/L), the main crystalline form of CC was calcite. But aragonite became dominant CC polymorph formed when the $MgCl_2$ concentration was increased to 0.025 M/L. Moreover, ACC was also formed, but its amount was rather small for quantification. The Mg^{2+} incorporated in ACC increased its stability and hindered its transformation from an amorphous phase to a crystalline phase [79, 80].

Another main carbonation product was an amorphous phase, which were characterized by ^{29}Si NMR and ^{27}Al NMR. The results indicated that Q^3 signal (at about -100 ppm) corresponding to the hydroxylated surface sites ($(SiO)_3$–Si-OH) and Q^4 signal (at about -110 ppm) corresponding to ($(SiO\text{-})_4Si$) in the alumina-silica gel and silica gel were formed (as shown in Figure 12). Also, the FTIR peaks at about 1038 cm^{-1} are linked to the vibration of Si-O bonds associated with the formation of silica gel according to previous studies [52, 67]. Moreover, the ^{27}Al NMR spectra in Figure 13 also demonstrated that aluminum was incorporated in the alumina-silica gel. Therefore, the main amorphous gels presence in the AWM were silica gel and alumina-silica gel.

The XRD results indicated that the calcium silicates including C_3S and C_2S were the most reactive components in cement (Figure 9). The carbonated products would be CC and silica bearing gel such as silica gel and alumina-silica gel. For the aluminum phase and iron phase in the cement, the carbonation of these two phase were confirmed by XRD and ^{27}Al NMR results, showing that the formation of alumina-silica gel was similar to the carbonation products of aluminum-bearing phases in the cement paste

including ettringite, AFm and C-A-S-H [46, 71, 81], which was contrary to the findings of a previous study [19]. It was possible that the dissolved aluminum and iron would also be incorporated in the silica bearing gel.

The formation of carbonation products and the evolution of the cement microstructure are illustrated in Figure 18. Firstly, brucite was formed in the solution and on the surface of the cement particles after mixing. Secondly, the brucite was rapidly consumed, while aragonite with a low length to diameter ratio and amorphous gel were formed on the cement particles. Thirdly, once brucite was completely disappeared after 30 min, both needle-like aragonite and amorphous gel grew on the cement particle. Finally, the cement grains were ruptured, and the individual aragonite whiskers could be observed at 120 min.

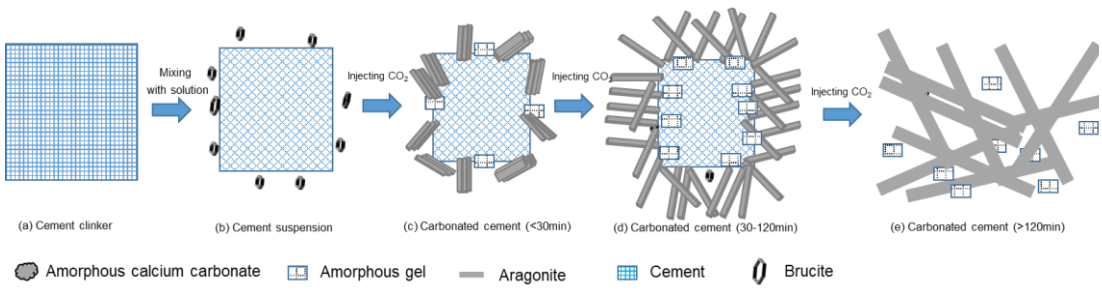

Figure 18 Formation of carbonation products and microstructure

5.1.2 Factors favoring aragonite formation

From the above results, temperature and $MgCl_2$ concentration are key factors controlling the aragonite formation during carbonation. From section 3.2, temperature seemed to be a key factor controlling the aragonite formation and its morphology. In general, the clusters of different-oriented aragonite started to form at 40 ℃, while the

aragonite crystals became needle-like at 80 ℃. The increased temperature not only promoted the aragonite formation but also affected its crystal growth direction and size. Usually, polymorph formations were controlled by their nucleation energies during the carbonation process [82]. In this study, the temperature mainly influenced the solubility product of CC and the dissolution of the anhydrous cement. Firstly, the solubility products of calcite and aragonite both increased with the increase of temperature, but the increase in the solubility of aragonite was higher than that of calcite, leading to a reduced difference in solubility products [82]. This might contribute to the nucleation of aragonite. Meanwhile, the higher temperature increased the activity of Mg^{2+} in solution, which rendered sufficient amount of Mg^{2+} located on the microcrystalline surface of calcite which restrained its nucleation and growth [64]. Furthermore, although the solubility of CO_2 was reduced under high temperature, the dissolution and precipitation processes were accelerated, consequently leading to a promoted carbonation rate.

Except temperature, magnesium concentration is another key factor affecting aragonite formation. In order to investigate the influence of magnesium concentration, the evolution of Mg^{2+} and Ca^{2+} ions in the suspension prepared with different initial $MgCl_2$ concentrations were measured and are shown in Figure 19. For all the samples, the Ca^{2+} concentration increased rapidly to the maximum values at 5 min before injecting CO_2, and then it decreased continually in the subsequent carbonation period. On the contrary, Mg^{2+} concentration showed an opposite trend. The increased Ca^{2+} and

reduced Mg^{2+} were attributed to the dissolution of cement and reaction between Mg^{2+} and the dissolved OH^-, which was confirmed by the formation of brucite. Therefore, a system of cement-$MgCl_2$-$Mg(OH)_2$-$CaCl_2$ was formed before injecting CO_2 (shown in Equation 5). It can be seen that the Ca^{2+} concentration increased with the increasing $MgCl_2$ concentration. When the initial concentration of $MgCl_2$ was lower than 0.01 M, the Mg^{2+} concentration was reduced to less than 0.5 ppm immediately after mixing with cement, indicating the exhaustion of $MgCl_2$ due to the excess OH^- dissolved from cement. Therefore, the suspension became a system of Cement-$Mg(OH)_2$-$CaCl_2$, preventing the formation of aragonite at an early age because only a limited amount of Mg^{2+} was present in solution. It is interesting to note that the concentration of Mg^{2+} increased and reached a relatively high value after injecting CO_2, which was attributed to the reaction shown in Equation 6. Meanwhile, Ca^{2+} showed an opposite trend. Afterwards, aragonite was formed again due to the increased Mg^{2+} concentration, which was evidenced by the changes of the amount of calcite and aragonite shown in the XRD results (samples carbonated in 0.01 M/L $MgCl_2$).

But for the samples carbonated in a lower $MgCl_2$ concentration, a lower amount of aragonite was obtained. It should be noted that the Ca^{2+} concentration changed associated with the evolution of Mg^{2+}. In order to further explore the effect of Mg^{2+}, the development Mg^{2+}/Ca^{2+} ratio calculated based on the ICP results, a minimum Mg^{2+}/Ca^{2+} ratio of 0.12 should be achieved before injecting CO_2 to ensure the formation of aragonite with needle-like morphology.

$$Ca(OH)_2 + MgCl_2 \rightarrow Mg(OH)_2 + CaCl_2 \quad (5)$$

$$CaCl_2 + CO_2 + Mg(OH)_2 \rightarrow CaCO_3 + H_2O + MgCl_2 \quad (6)$$

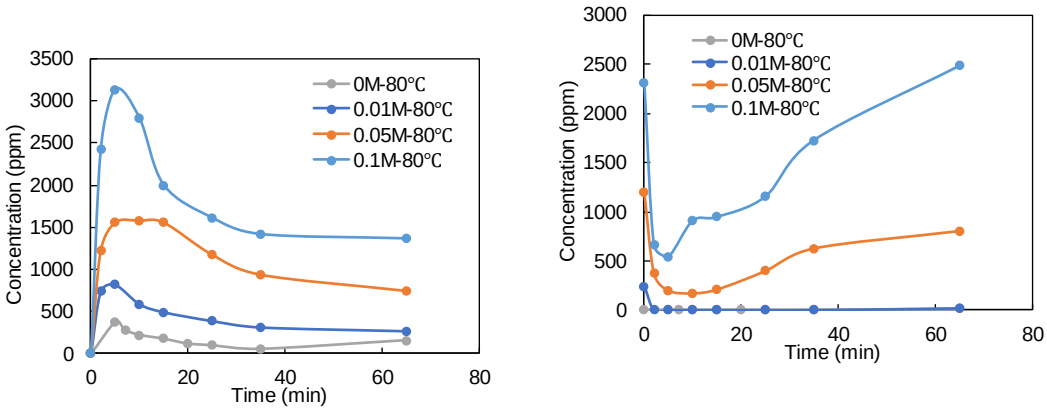

(a) The development of Ca^{2+} (b) The development of Mg^{2+}

Figure 19 Development of Ca^{2+} and Mg^{2+} during carbonation

5.2 Enhanced mechanical properties and accelerated hydration of micro-fiber reinforced cement

In this study, it has been proven that the AWM addition led to the accelerated hydration, resulting in increased compressive strength and flexural strength at both early and later ages. This was not only attributed to the high reactivity of AWM, but also contributed by the additional nucleation sites, refinement effects, and fiber bridging effect induced by the incorporation of AWM.

Firstly, the higher early strength was attributed to the high reactivity of AWM, as the high reactivity of AWM was related to the presence of the amorphous gels, which might have similar characteristics to silica fume as revealed by NMR results in Figure 12 and 13. In addition, the prepared AWM had a very high BET surface area (>23 m^2/g while only 1.70 m^2/g for Portland cement. This significantly increased surface area was

due to the formation of amorphous phases from the decalcified clinker. This BET surface area was even higher than that of metakaolin and silica fume [83, 84]. As a result, the AWM would react with $Ca(OH)_2$ and promote the reaction of the silicate phases. Then, the high reactivity of AWM had a noticeable influence on cement hydration and contributed to the enhanced mechanical properties.

Secondly, the amorphous phases in AWM possessed a high surface area, it would work both as nucleation sites accelerating the cement hydration and a supplementary cementing material (pozzolanic material), resulting in pore refinement effect [85]. Also, it has been reported that aragonite can provide additional nucleation sites, promoting the precipitation of hydration products and accelerating the hydration of cement [76]. As a result, an accelerated hydration rate and a higher hydration degree were recorded, resulting in increased compressive strength and flexural strength at both the early and later ages.

Thirdly, the needle-like aragonite whiskers with crystalline particle lengths of 10-30 μm and diameters of 0.5-2 μm were synthesized, which could serve as micro-fibers to arrest crack growth in cement paste [86]. As a result, an increased mechanical property of micro-fiber reinforced cement could be observed.

5.3 CO_2 sequestration and reduction by the use of micro-fiber reinforced cement

Based on the above test results, an appreciable amount of CO_2 participated in the formation of AWM by the wet carbonation process. The amounts of carbonation

products and CO_2 sequestration were calculated based on the results from XRD, TG and weighting after carbonation. The results showed that about 0.413 g of CO_2 was sequestrated by 1 g of cement after carbonation for 120 min, generating around 1.519 g of AWM.

As when using the aragonite whisker as micro-fiber and the amorphous gel as ultra-fine and ultra-reactive supplementary cementitious materials, the amount of clinker in cement can be reduced which would in turn reduce embodied carbon in the concrete product [87]. The potential CO_2 reduction is summarized in Figure 20 (assuming a 20 % replacement of clinker content is adopted). Another reduction of 20 % CO_2 emission would be achieved from the reduced content of clinker [88]. As the previous study shows that about 1 ton CO_2 was consumed for the production of 1ton of clinker in Hong Kong [89]. Thus, a CO_2 reduction of 5.3 % would be obtained due to the CO_2 sequestration in AWM. According to the above analysis, a CO_2 emission reduction of more than 25.3 % could acquire during the cement production.

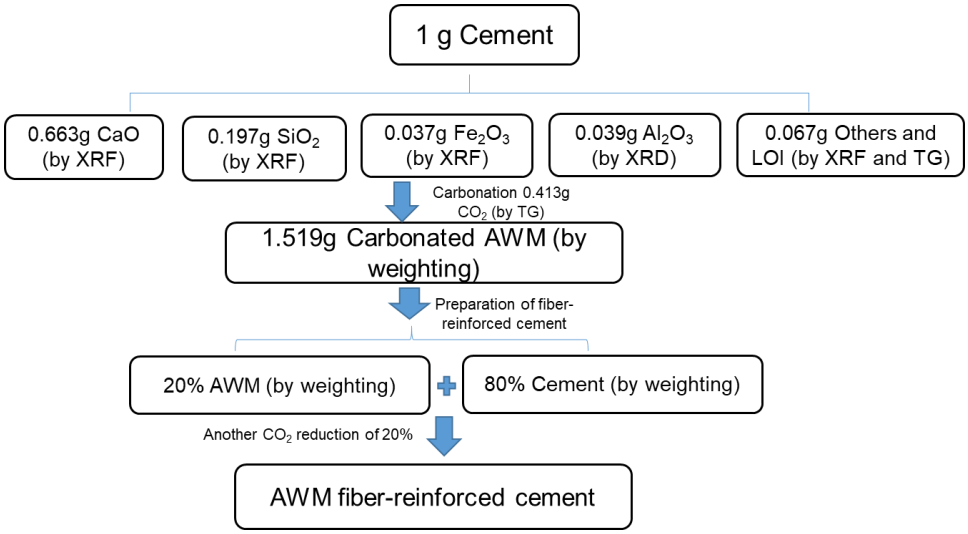

Figure 20 Potential CO_2 reduction of the micro-fiber reinforced cement

5.4 Benefits of this study

The world is facing a great environmental challenge due to the extensive release of CO_2. To mitigate global warming and associated climate changes, sequestering CO_2 by cement based materials has attracted a lot of interests. The carbonation of cement based materials has been investigated for many years, and the generation of different polymorphs of calcium carbonate including calcite, aragonite, vaterite and amorphous calcium carbonate could be observed. But the relative amounts of these polymorphs formed varied from different studies. Only a few research studies mentioned controlling the polymorph of calcium carbonate during the carbonation of cement based materials. Considering the morphologies and characteristics of different polymorphs, the production of aragonite by inhibiting the transformation from aragonite to calcite is of great interest for high-value utilization of cement based materials by using accelerated

carbonation. In this study, a production process for needle-like AWM was developed through the carbonation of Portland cement, while the temperature and $MgCl_2$ addition's concentration were precisely controlled, and the production mechanism was revealed.

The proposed approach is a novel way of preparing an aragonite whisker-rich material by using cement clinkers and flue gas in the cement plant, which has a great potential to be upscaled. This approach tackles several issues at the same time: 1) The direct utilize of flue gas, which provides a feasible way to reduce CO_2 emission in cement plants and helps to make cement and concrete production "greener" in terms of CO_2 emissions; 2) Preparation of value-added products (aragonite whisker-rich materials) within one hour of wet carbonation, that can be used in many applications; 3) Revealing the carbonation mechanisms of the formation of AWM, which is of great importance for controlling the carbonation products, regulating the formation of polymorphs of calcium carbonate and expanding our understanding on the kinetics of carbonation of cement based materials; 4) Preparation of micro-fiber reinforced cement in cement plants, which possesses very high mechanical properties and cracking resistance.

6. Conclusion

In this study, a novel way of preparing needle-like AWM by using cement clinkers and flue gas in the cement plant was developed by simultaneously controlling the

temperature and $MgCl_2$ concentration. This study provides a way to reduce CO_2 emission in cement plant and helps to make cement and concrete production more "green" in terms of CO_2 emission. Based on the experimental results, the following conclusions can be drawn.

(1) Needle-like aragonite whiskers with single crystal lengths of 10-30 μm and diameter of 0.5-2 μm could be synthesized rapidly when the CO_2 was injected into a cement suspension with 0.05 M $MgCl_2$ at 80 ℃.

(2) The prepared AWM consisting of aragonite and amorphous phases were prepared rapidly by the wet carbonation process.

(3) The AWM addition led to the accelerated hydration and a higher hydration degree of cement when it was added to a new cement, and as a result, micro-fiber reinforced cement was prepared by mixing AWM and Portland cement, which showed significant improvement in compressive strength (up to 24.1 % increase) and flexural strength (up to 25.9 % increase). Meanwhile, compared to conventional OPC production, this newly developed cement exhibited a significantly lower embodied carbon.

(4) The proposed wet carbonation route was able to sequestrate 0.413 g CO_2/g cement and the whole process could complete rapidly. Also, it is expected that it can be easily up-scaled and adopted in cement plants, since both cement and CO_2 can be sourced together.

(5) Temperature and magnesium ion concentration were the main key factors

affecting the formation of aragonite whiskers. Therein, the increased temperature improved the activity of magnesium ions which rendered sufficient Mg^{2+} located on the microcrystal surface of calcite and restrained the nucleation and growth of calcite. Aragonite whiskers preferred to form in the system of cement-$MgCl_2$-$Mg(OH)_2$-$CaCl_2$ with a high Ca^{2+} concentration and a minimum Mg^{2+}/Ca^{2+} molar ratio of higher than 0.12.

(6) Amorphous phases including silica gel and alumina-silica gel were formed, which had high pozzolanic reactivity and contributed to the improved performance of the micro-fiber reinforced cement.

Acknowledgements

The authors wish to acknowledge the financial supports of the Research Grant Council (GRF), the Construction Industry Council and the Strategic Public Policy Research (SPPR) Funding Scheme for financial support. We also gratefully acknowledge the equipment support of the University Research Facility on Chemical and Environmental Analysis (URFCE) of PolyU.

Reference

[1] J.G. Olivier, J.A. Peters, G. Janssens-Maenhout, Trends in global CO2 emissions. 2012 report, (2012).

[2] N. Rodriguez, R. Murillo, M. Alonso, I. Martinez, G. Grasa, J. Abanades, Analysis of a process for capturing the CO2 resulting from the precalcination of limestone in a cement plant, Industrial & engineering chemistry research, 50 (2011) 2126-2132.

[3] A. Hasanbeigi, L. Price, E. Lin, Emerging energy-efficiency and CO2 emission-reduction technologies for cement and concrete production: A technical review, Renewable and Sustainable Energy Reviews, 16 (2012) 6220-6238.

[4] H. Gante Caruso, Reduction of CO2 emissions from cement plants, University of Waterloo, 2007.

[5] M.G. Plaza, S. Martínez, F. Rubiera, CO2 Capture, use, and Storage in the Cement Industry: State of the Art and Expectations, Energies, 13 (2020) 5692.

[6] J. Jakobsen, S. Roussanaly, R. Anantharaman, A techno-economic case study of CO2 capture, transport and storage chain from a cement plant in Norway, Journal of cleaner production, 144 (2017) 523-539.

[7] K. Vatopoulos, E. Tzimas, Assessment of CO2 capture technologies in cement manufacturing process, Journal of cleaner production, 32 (2012) 251-261.

[8] D. Barker, S. Turner, P. Napier-Moore, M. Clark, J. Davison, CO2 capture in the cement industry, Energy procedia, 1 (2009) 87-94.

[9] J. Morrison, G. Jauffret, J.L. Galvez-Martos, F.P. Glasser, Magnesium-based cements for CO2 capture and utilisation, Cement and Concrete Research, 85 (2016) 183-191.

[10] I. In, B. Metz, O. Davidson, H. Coninck, M. Loos, L. Meyer, Special Report on Carbon Dioxide Capture and Storage, Metz, B., Davidson, O., Coninck, HC, Loos, M., Meyer, LA, Eds, (2005).

[11] T. Hills, D. Leeson, N. Florin, P. Fennell, Carbon capture in the cement industry: technologies, progress, and retrofitting, Environmental science & technology, 50 (2016) 368-377.

[12] S. Roussanaly, C. Fu, M. Voldsund, R. Anantharaman, M. Spinelli, M. Romano, Techno-economic analysis of MEA CO2 capture from a cement kiln–impact of steam supply scenario, Energy Procedia, 114 (2017) 6229-6239.

[13] K. Lindqvist, S. Roussanaly, R. Anantharaman, Multi-stage membrane processes for CO2 capture from cement industry, Energy Procedia, 63 (2014) 6476-6483.

[14] M. Diego, B. Arias, J. Abanades, Analysis of a double calcium loop process configuration for CO2 capture in cement plants, Journal of Cleaner Production, 117 (2016) 110-121.

[15] M. Hornberger, R. Spörl, G. Scheffknecht, Calcium looping for CO2 capture in cement plants–pilot scale test, Energy Procedia, 114 (2017) 6171-6174.

[16] S.O. Gardarsdottir, E. De Lena, M. Romano, S. Roussanaly, M. Voldsund, J.-F. Pérez-Calvo, D. Berstad, C. Fu, R. Anantharaman, D. Sutter, Comparison of technologies for CO2 capture from cement production—Part 2: Cost analysis, Energies, 12 (2019) 542.

[17] S. Kashef-Haghighi, S. Ghoshal, CO2 sequestration in concrete through accelerated carbonation curing in a flow-through reactor, Industrial & engineering chemistry research, 49 (2010) 1143-1149.

[18] Y. Shao, Beneficial Use of Carbon Dioxide in Precast Concrete Production, McGill Univ., Montreal, QC (Canada), 2014.

[19] M. Zajac, A. Lechevallier, P. Durdzinski, F. Bullerjahn, J. Skibsted, M. Ben Haha, CO2 mineralisation of Portland cement: Towards understanding the mechanisms of enforced carbonation, Journal of CO2 Utilization, 38 (2020) 398-415.

[20] W. Ashraf, J. Olek, Carbonation behavior of hydraulic and non-hydraulic calcium silicates: potential of utilizing low-lime calcium silicates in cement-based materials, Journal of Materials Science, 51 (2016) 6173-6191.

[21] O. Shtepenko, C. Hills, A. Brough, M. Thomas, The effect of carbon dioxide on β-dicalcium silicate and Portland cement, Chemical Engineering Journal, 118 (2006) 107-118.

[22] S. Goto, K. Suenaga, T. Kado, M. Fukuhara, Calcium silicate carbonation products, Journal of the American Ceramic Society, 78 (1995) 2867-2872.

[23] G. Wolf, C. Günther, Thermophysical investigations of the polymorphous phases of calcium carbonate, Journal of thermal analysis and calorimetry, 65 (2001) 687-698.

[24] Z. Hu, M. Shao, Q. Cai, S. Ding, C. Zhong, X. Wei, Y. Deng, Synthesis of needle-like aragonite from limestone in the presence of magnesium chloride, Journal of materials processing technology, 209 (2009) 1607-1611.

[25] M. Cao, C. Zhang, H. Lv, L. Xu, Characterization of mechanical behavior and mechanism of calcium carbonate whisker-reinforced cement mortar, Construction and Building Materials, 66 (2014) 89-97.

[26] M. Cao, L. Li, L. Xu, Relations between rheological and mechanical properties of fiber reinforced mortar, Comput. Concr, 20 (2017) 449-459.

[27] N. Banthia, F. Majdzadeh, J. Wu, V. Bindiganavile, Fiber synergy in Hybrid Fiber Reinforced Concrete (HyFRC) in flexure and direct shear, Cement and Concrete Composites, 48 (2014) 91-97.

[28] X. Luo, W. Sun, S.Y.N. Chan, Effect of heating and cooling regimes on residual strength and microstructure of normal strength and high-performance concrete, Cement and Concrete Research, 30 (2000) 379-383.

[29] B. Wang, Y. Han, S. Liu, Effect of highly dispersed carbon nanotubes on the flexural toughness of cement-based composites, Construction and Building Materials, 46 (2013) 8-12.

[30] T. Han, H. Wang, X. Jin, J. Yang, Y. Lei, F. Yang, X. Yang, Z. Tao, Q. Guo, L. Liu, Multiscale carbon nanosphere–carbon fiber reinforcement for cement-based

composites with enhanced high-temperature resistance, Journal of Materials Science, 50 (2015) 2038-2048.

[31] J. Lawler, T. Wilhelm, D. Zampini, S. Shah, Fracture processes of hybrid fiber-reinforced mortar, Materials and Structures, 36 (2003) 197-208.

[32] N. Banthia, A. Moncef, K. Chokri, J. Sheng, Uniaxial tensile response of microfibre reinforced cement composites, Materials and Structures, 28 (1995) 507-517.

[33] M. Cao, J. Wei, Microstructure and mechanical properties of CaCO 3 whisker-reinforced cement, Journal of Wuhan University of Technology-Mater. Sci. Ed., 26 (2011) 1004-1009.

[34] A. Sivakumar, M. Santhanam, Mechanical properties of high strength concrete reinforced with metallic and non-metallic fibres, Cement and Concrete Composites, 29 (2007) 603-608.

[35] H. Yazıcı, M.Y. Yardımcı, H. Yiğiter, S. Aydın, S. Türkel, Mechanical properties of reactive powder concrete containing high volumes of ground granulated blast furnace slag, Cement and Concrete Composites, 32 (2010) 639-648.

[36] F. Tuba, L. Oláh, P. Nagy, Characterization of the fracture properties of aragonite‐and calcite‐filled poly (ε‐caprolactone) by the essential work of fracture method, Journal of applied polymer science, 120 (2011) 2587-2595.

[37] L. Li, M. Cao, H. Yin, Comparative roles between aragonite and calcite calcium carbonate whiskers in the hydration and strength of cement paste, Cement and Concrete Composites, 104 (2019) 103350.

[38] H. Ma, J. Cai, Z. Lin, S. Qian, V.C. Li, CaCO3 whisker modified Engineered Cementitious Composite with local ingredients, Construction and Building Materials, 151 (2017) 1-8.

[39] M. Li, Y. Yang, M. Liu, X. Guo, S. Zhou, Hybrid effect of calcium carbonate whisker and carbon fiber on the mechanical properties and microstructure of oil well cement, Construction and Building Materials, 93 (2015) 995-1002.

[40] S.A. Bernal, J.L. Provis, B. Walkley, R. San Nicolas, J.D. Gehman, D.G. Brice, A.R. Kilcullen, P. Duxson, J.S. van Deventer, Gel nanostructure in alkali-activated binders based on slag and fly ash, and effects of accelerated carbonation, Cement and Concrete Research, 53 (2013) 127-144.

[41] S.A. Bernal, J.L. Provis, D.G. Brice, A. Kilcullen, P. Duxson, J.S. van Deventer, Accelerated carbonation testing of alkali-activated binders significantly underestimates service life: The role of pore solution chemistry, Cement and Concrete Research, 42 (2012) 1317-1326.

[42] S.A. Bernal, R. San Nicolas, R.J. Myers, R.M. de Gutiérrez, F. Puertas, J.S. van Deventer, J.L. Provis, MgO content of slag controls phase evolution and structural changes induced by accelerated carbonation in alkali-activated binders, Cement and Concrete Research, 57 (2014) 33-43.

[43] A.E. Morandeau, C.E. White, Role of magnesium-stabilized amorphous calcium carbonate in mitigating the extent of carbonation in alkali-activated slag, Chemistry of Materials, 27 (2015) 6625-6634.

[44] D. Gebauer, A. Völkel, H. Cölfen, Stable prenucleation calcium carbonate clusters, Science, 322 (2008) 1819-1822.
[45] W. Ashraf, J. Olek, Elucidating the accelerated carbonation products of calcium silicates using multi-technique approach, Journal of CO2 Utilization, 23 (2018) 61-74.
[46] M. Auroy, S. Poyet, P. Le Bescop, J.-M. Torrenti, T. Charpentier, M. Moskura, X. Bourbon, Comparison between natural and accelerated carbonation (3% CO2): Impact on mineralogy, microstructure, water retention and cracking, Cement and Concrete Research, 109 (2018) 64-80.
[47] R.I. Khan, W. Ashraf, J. Olek, Amino acids as performance-controlling additives in carbonation-activated cementitious materials, Cement and Concrete Research, 147 (2021) 106501.
[48] S. Zhao, Z. Liu, Y. Mu, F. Wang, Y. He, Effect of chitosan on the carbonation behavior of γ-C2S, Cement and Concrete Composites, 111 (2020) 103637.
[49] Z. Hu, M. Shao, H. Li, Q. Cai, C. Zhong, Z. Xianming, Y. Deng, Synthesis of needle-like aragonite crystals in the presence of magnesium chloride and their application in papermaking, Advanced composite materials, 18 (2009) 315-326.
[50] Y. Ota, S. Inui, T. Iwashita, T. KASUGA, Y. ABE, Preparation conditions for aragonite whiskers by carbonation process, Journal of the Ceramic Society of Japan, 104 (1996) 196-200.
[51] P. He, B. Zhang, J.-X. Lu, C.S. Poon, ASR expansion of alkali-activated cement glass aggregate mortars, Constr. Build. Mater., 261 (2020) 119925.
[52] M. Zajac, J. Skibsted, P. Durdzinski, F. Bullerjahn, J. Skocek, M. Ben Haha, Kinetics of enforced carbonation of cement paste, Cement and Concrete Research, 131 (2020) 106013.
[53] Z. Zou, L. Bertinetti, Y. Politi, A.C.S. Jensen, S. Weiner, L. Addadi, P. Fratzl, W.J.E.M. Habraken, Opposite Particle Size Effect on Amorphous Calcium Carbonate Crystallization in Water and during Heating in Air, Chemistry of Materials, 27 (2015) 4237-4246.
[54] C. Günther, A. Becker, G. Wolf, M. Epple, In vitro synthesis and structural characterization of amorphous calcium carbonate, Zeitschrift für anorganische und allgemeine Chemie, 631 (2005) 2830-2835.
[55] L. Fernández-Carrasco, D. Torrens-Martín, L. Morales, S. Martínez-Ramírez, Infrared spectroscopy in the analysis of building and construction materials, Infrared spectroscopy–Materials science, engineering and technology, (2012) 369-382.
[56] I.S. Del Bosque, S. Martínez-Ramírez, M.T. Blanco-Varela, FTIR study of the effect of temperature and nanosilica on the nano structure of C–S–H gel formed by hydrating tricalcium silicate, Construction and Building Materials, 52 (2014) 314-323.
[57] Y. Politi, D.R. Batchelor, P. Zaslansky, B.F. Chmelka, J.C. Weaver, I. Sagi, S. Weiner, L. Addadi, Role of magnesium ion in the stabilization of biogenic amorphous calcium carbonate: A structure− function investigation, Chemistry of Materials, 22 (2010) 161-166.

[58] J. Jiang, M.-R. Gao, Y.-H. Qiu, S.-H. Yu, Gram-scale, low-cost, rapid synthesis of highly stable Mg–ACC nanoparticles and their long-term preservation, Nanoscale, 2 (2010) 2358-2361.

[59] S. Liu, H. Zhang, Y. Wang, M. Gou, Carbon-dioxide-activated bonding material with low water demand, Advances in Cement Research, (2020) 1-4.

[60] S. Liu, X. Guan, H. Zhang, Y. Wang, M. Gou, Revealing the Microstructure Evolution and Carbonation Hardening Mechanism of β-C2S Pastes by Backscattered Electron Images, Materials, 12 (2019) 1561.

[61] C. Liu, T. Liu, D. Wang, Non-isothermal kinetics study on the thermal decomposition of brucite by thermogravimetry, Journal of Thermal Analysis and Calorimetry, 134 (2018) 2339-2347.

[62] H. Ren, Z. Chen, Y. Wu, M. Yang, J. Chen, H. Hu, J. Liu, Thermal characterization and kinetic analysis of nesquehonite, hydromagnesite, and brucite, using TG–DTG and DSC techniques, Journal of Thermal Analysis and Calorimetry, 115 (2014) 1949-1960.

[63] Q. Huang, G. Lu, J. Wang, J. Yu, Thermal decomposition mechanisms of MgCl2· 6H2O and MgCl2· H2O, Journal of Analytical and Applied Pyrolysis, 91 (2011) 159-164.

[64] N. Yamaguchi, Y. Masuda, Y. Yamada, H. Narusawa, C. Han-Cheol, Y. Tamaki, T. Miyazaki, Synthesis of CaO-SiO 2 Compounds Using Materials Extracted from Industrial Wastes, Open Journal of Inorganic Non-Metallic Materials, 5 (2014) 1.

[65] A. Radha, T.Z. Forbes, C.E. Killian, P. Gilbert, A. Navrotsky, Transformation and crystallization energetics of synthetic and biogenic amorphous calcium carbonate, Proceedings of the National Academy of Sciences, 107 (2010) 16438-16443.

[66] J. Zhang, X. Zhou, C. Dong, Y. Sun, J. Yu, Investigation of amorphous calcium carbonate's formation under high concentration of magnesium: The prenucleation cluster pathway, Journal of Crystal Growth, 494 (2018) 8-16.

[67] S. Liu, J. Wang, H. Zhang, X. Guan, M. Qiu, Z. Dou, Microstructure of β-Dicalcium Silicate after Accelerated Carbonation, Journal of Wuhan University of Technology-Mater. Sci. Ed., 34 (2019) 122-126.

[68] A.G. P Colombet, H Zanni, P Sozzani, Nuclear magnetic resonance spectroscopy of cement-based materials, 2012.

[69] T.F. Sevelsted, J. Skibsted, Carbonation of C–S–H and C–A–S–H samples studied by 13C, 27Al and 29Si MAS NMR spectroscopy, Cement and concrete Research, 71 (2015) 56-65.

[70] J. Chang, Y. Fang, X. Shang, The role of β-C2S and γ-C2S in carbon capture and strength development, Materials and Structures, 49 (2016) 4417-4424.

[71] T.F. Sevelsted, J. Skibsted, Carbonation of C–S–H and C–A–S–H samples studied by 13 C, 27 Al and 29 Si MAS NMR spectroscopy, Cement and Concrete Research, 71 (2015) 56-65.

[72] P. Shen, L. Lu, W. Chen, F. Wang, S. Hu, Efficiency of metakaolin in steam cured high strength concrete, Construction and Building Materials, 152 (2017) 357-366.

[73] J.F. Stebbins, Nuclear magnetic resonance spectroscopy of silicates and oxides in geochemistry and geophysics, Handbook of physical constants, 2 (1995) 303-332.

[74] M.I. Macedo, C.C. Osawa, C.A. Bertran, Sol-gel synthesis of transparent alumina gel and pure gamma alumina by urea hydrolysis of aluminum nitrate, Journal of sol-gel science and technology, 30 (2004) 135-140.

[75] M. Zajac, J. Skocek, P. Durdzinski, F. Bullerjahn, J. Skibsted, M.B. Haha, Effect of carbonated cement paste on composite cement hydration and performance, Cement and Concrete Research, 134 (2020) 106090.

[76] D.P. Bentz, A. Ardani, T. Barrett, S.Z. Jones, D. Lootens, M.A. Peltz, T. Sato, P.E. Stutzman, J. Tanesi, W.J. Weiss, Multi-scale investigation of the performance of limestone in concrete, Construction and Building Materials, 75 (2015) 1-10.

[77] B. Bissonnette, M. Pigeon, Tensile creep at early ages of ordinary, silica fume and fiber reinforced concretes, Cement and Concrete Research, 25 (1995) 1075-1085.

[78] X. Ouyang, L. Wang, S. Xu, Y. Ma, G. Ye, Surface characterization of carbonated recycled concrete fines and its effect on the rheology, hydration and strength development of cement paste, Cement and Concrete Composites, 114 (2020) 103809.

[79] E. Loste, R.M. Wilson, R. Seshadri, F.C. Meldrum, The role of magnesium in stabilising amorphous calcium carbonate and controlling calcite morphologies, Journal of Crystal growth, 254 (2003) 206-218.

[80] T. Ogino, T. Suzuki, K. Sawada, The formation and transformation mechanism of calcium carbonate in water, Geochimica et Cosmochimica Acta, 51 (1987) 2757-2767.

[81] M. Zajac, J. Skibsted, J. Skocek, P. Durdzinski, F. Bullerjahn, M. Ben Haha, Phase assemblage and microstructure of cement paste subjected to enforced, wet carbonation, Cement and Concrete Research, 130 (2020) 105990.

[82] L.N. Plummer, E. Busenberg, The solubilities of calcite, aragonite and vaterite in CO2-H2O solutions between 0 and 90 C, and an evaluation of the aqueous model for the system CaCO3-CO2-H2O, Geochimica et cosmochimica acta, 46 (1982) 1011-1040.

[83] P. Shen, L. Lu, Y. He, F. Wang, S. Hu, The effect of curing regimes on the mechanical properties, nano-mechanical properties and microstructure of ultra-high performance concrete, Cement and Concrete Research, 118 (2019) 1-13.

[84] M. Zajac, P. Durdzinski, C. Stabler, J. Skocek, D. Nied, M.B. Haha, Influence of calcium and magnesium carbonates on hydration kinetics, hydrate assemblage and microstructural development of metakaolin containing composite cements, Cement and Concrete Research, 106 (2018) 91-102.

[85] L.P. Singh, S.R. Karade, S.K. Bhattacharyya, M.M. Yousuf, S. Ahalawat, Beneficial role of nanosilica in cement based materials – A review, Construction and Building Materials, 47 (2013) 1069-1077.

[86] R. Talreja, Matrix and fiber–matrix interface cracking in composite materials, Modeling Damage, Fatigue and Failure of Composite Materials, Elsevier2016, pp. 87-96.

[87] H. Klee, Briefing: The Cement Sustainability Initiative, Proceedings of the Institution of Civil Engineers-Engineering Sustainability, Thomas Telford Ltd, 2004, pp. 9-11.

[88] R. Rosković, D. Bjegović, Role of mineral additions in reducing CO2 emission, Cement and Concrete Research, 35 (2005) 974-978.

[89] J. Zhang, J.C. Cheng, I.M. Lo, Life cycle carbon footprint measurement of Portland cement and ready mix concrete for a city with local scarcity of resources like Hong Kong, The international journal of life cycle assessment, 19 (2014) 745-757.